Sedimentary Geology 362 (2017) 83–100

Contents lists available at ScienceDirect

Sedimentary Geology

journal homepage: www.elsevier.com/locate/sedgeo

3D architecture of cyclic-step and antidune deposits in glacigenic subaqueous fan and delta settings: Integrating outcrop and ground-penetrating radar data

Jörg Lang [a,*], Julian Sievers [a], Markus Loewer [b], Jan Igel [b], Jutta Winsemann [a]

[a] Institut für Geologie, Leibniz Universität Hannover, Callinstraße 30, 30167 Hannover, Germany
[b] Leibniz Institute for Applied Geophysics (LIAG), Stilleweg 2, 30655 Hannover, Germany

ARTICLE INFO

Article history:
Received 27 July 2017
Received in revised form 23 October 2017
Accepted 24 October 2017
Available online 28 October 2017

Editor: Dr. J. Knight

Keywords:
Cyclic steps
Antidunes
Supercritical density flow
Ground-penetrating radar
Subaqueous ice-contact fan
Glacifluvial delta

ABSTRACT

Bedforms related to supercritical flows are increasingly recognised as important constituents of many depositional environments, but outcrop studies are commonly hampered by long bedform wavelengths and complex three-dimensional geometries. We combined outcrop-based facies analysis with ground-penetrating radar (GPR) surveys to analyse the 3D facies architecture of subaqueous ice-contact fan and glacifluvial delta deposits. The studied sedimentary systems were deposited at the margins of the Middle Pleistocene Scandinavian ice sheets in Northern Germany.

Glacifluvial Gilbert-type deltas are characterised by steeply dipping foreset beds, comprising cyclic-step deposits, which alternate with antidune deposits. Deposits of cyclic steps consist of lenticular scours infilled by backset cross-stratified pebbly sand and gravel. The GPR sections show that the scour fills form trains along the delta foresets, which can locally be traced for up to 15 m. Perpendicular and oblique to palaeoflow direction, these deposits appear as troughs with concentric or low-angle cross-stratified infills. Downflow transitions from scour fills into sheet-like low-angle cross-stratified or sinusoidally stratified pebbly sand, deposited by antidunes, are common. Cyclic steps and antidunes were deposited by sustained and surge-type supercritical density flows, which were related to hyperpycnal flows, triggered by major meltwater discharge or slope-failure events.

Subaqueous ice-contact fan deposits include deposits of progradational scour fills, isolated hydraulic jumps, antidunes and (humpback) dunes. The gravel-rich fan succession consists of vertical stacks of laterally amalgamated pseudo-sheets, indicating deposition by pulses of waning supercritical flows under high aggradation rates. The GPR sections reveal the large-scale architecture of the sand-rich fan succession, which is characterised by lobe elements with basal erosional surfaces associated with scours filled with backsets related to hydraulic jumps, passing upwards and downflow into deposits of antidunes and (humpback) dunes. The recurrent facies architecture of the lobe elements and their prograding and retrograding stacking pattern are interpreted as related to autogenic flow morphodynamics.

1. Introduction

Bedforms related to supercritical flows, including antidunes, chutes-and-pools and cyclic steps, have recently received much interest and have been identified as important constituents of depositional environments such as deltas (Ventra et al. 2015; Dietrich et al. 2016; Normandeau et al. 2016; Massari 2017), submarine fans (Postma et al. 2014; Ventra et al. 2015; Covault et al. 2017; Lang et al. 2017), and subaqueous ice-contact fans (Russell and Arnott 2003; Winsemann et al. 2009; Lang and Winsemann 2013). The understanding of the morphodynamics of supercritical flows has been greatly advanced by numerical and analogue modelling (Alexander et al. 2001; Kostic 2011, 2014; Cartigny et al. 2014; Fedele et al. 2017; Vellinga et al. 2017).

Supercritical flows are characterised by the dominance of inertial over gravitational forces and are defined by Froude numbers (*Fr*) larger than unity. For density flows, the densimetric Froude number Fr' is given by $Fr' = \bar{U}/\sqrt{(g'h)}$, where $\bar{U}$ is the mean flow velocity, h is the flow depth and g' is the reduced acceleration by gravity with $g' = g(\rho_f - \rho_w) / \rho_f$, where ρ_f is the density of the flow and ρ_w is the density of the ambient water. Supercritical flows over mobile sediment beds are characterised by in-phase relationships between disturbances of the upper, free flow surface and the morphology of the sediment-flow interface, and produce a range of bedforms, including stable and unstable antidunes, chutes-and-pools and cyclic steps (Hand 1974; Cartigny et al. 2014; Fedele et al. 2017). Besides the main controlling factors of

* Corresponding author.
E-mail address: lang@geowi.uni-hannover.de (J. Lang).

https://doi.org/10.1016/j.sedgeo.2017.10.011

flow velocity and density, the formation of different bedforms may also reflect variations in flow density, grain size and the ratio of bedload and suspended load (Spinewine et al. 2009; Kostic et al. 2010; Cartigny et al. 2014; Fedele et al. 2017). Deposits of supercritical flows are commonly characterised by lateral and vertical transitions between the various bedform types due to spatio-temporal variations of the flow conditions and feedbacks between the flow and the developing bedform (Spinewine et al. 2009; Kostic 2011, 2014; Cartigny et al. 2014; Zhong et al. 2015). Such facies changes may complicate the depositional architecture of the resulting bedforms.

Glacigenic depositional environments are commonly characterised by high-energy, sediment-laden, rapidly waning meltwater flows, and thus favour the occurrence of aggradational supercritical flows and the preservation of bedforms. Outcrop examples from Pleistocene glacilacustrine delta and subaqueous ice-contact fan successions indicate that deposits of such flows are characteristic of these depositional systems (Russell and Arnott 2003; Hornung et al. 2007; Winsemann et al. 2007, 2009, 2011; Lang and Winsemann 2013; Dietrich et al. 2016).

Subaqueous ice-contact fans are deposited by meltwater jets discharging from conduits at the grounding line of a glacier into a standing water body. Such plane-wall jet flows are characterised by a distinct proximal to distal zonation within the flows and the resulting deposits due to the expansion and deceleration by the entrainment of ambient water (Bates 1953; Powell 1990; Hoyal et al. 2003; Russell and Arnott 2003). These high-energy flows build a fan-shaped mouth bar that develops downflow of a flute-like scour and can be considered as a basic example of deposition by jet flows (Powell 1990; Russell and Arnott 2003; Hornung et al. 2007; Winsemann et al. 2009). The extent and geometry of jet flows and their deposits are controlled by the conduit diameter and Froude number (Powell 1990; Hoyal et al. 2003). On the lee side of the mouth bar, jet flows evolve into sustained density flows, allowing for basinwards sediment transport (Powell 1990; Lang et al. 2012; Dowdeswell et al. 2015).

Glacifluvial Gilbert-type deltas are fed by the discharge of meltwater streams and are characterised by a separation of the ice margin and the lake by a subaerial delta plain (Lønne 1995). Sediment is transferred towards the delta front and foot zones by a variety of sediment-gravity flow processes, including debris fall, debris flows and turbidity currents. Because the density of sediment-laden meltwater is commonly higher than the density of the ambient lake water, the development of hyperpycnal underflows is common (Ashley 1995; Lønne and Nemec 2004; Winsemann et al. 2007, 2011).

The aim of this study is to present new insights into the 2D and 3D depositional architecture of deposits related to supercritical flows in glacilacustrine environments. The observed bedforms and their lateral and vertical successions are interpreted in terms of the spatio-temporal evolution of the formative flows and linked to the larger-scale depositional architecture of the studied sections. Outcrop studies of bedforms related to supercritical flows are commonly hampered by their long wavelengths. Furthermore, most outcrop sections only allow for a limited analysis of the three-dimensional architecture of the deposits. Therefore, we combined outcrop-based facies analysis with extensive ground-penetrating radar (GPR) surveys. Different GPR antennas (200, 400 and 1500 MHz) were utilised to acquire both long profiles and densely spaced grids to map the large-scale facies architecture and image the high-resolution three-dimensional geometry of these deposits.

2. Study area

The study area is located in northern Germany (Fig. 1A). During the Middle Pleistocene Saalian glaciation (Marine Isotope Stage 6) the advances of the Scandinavian ice sheets led to the blocking of the drainage

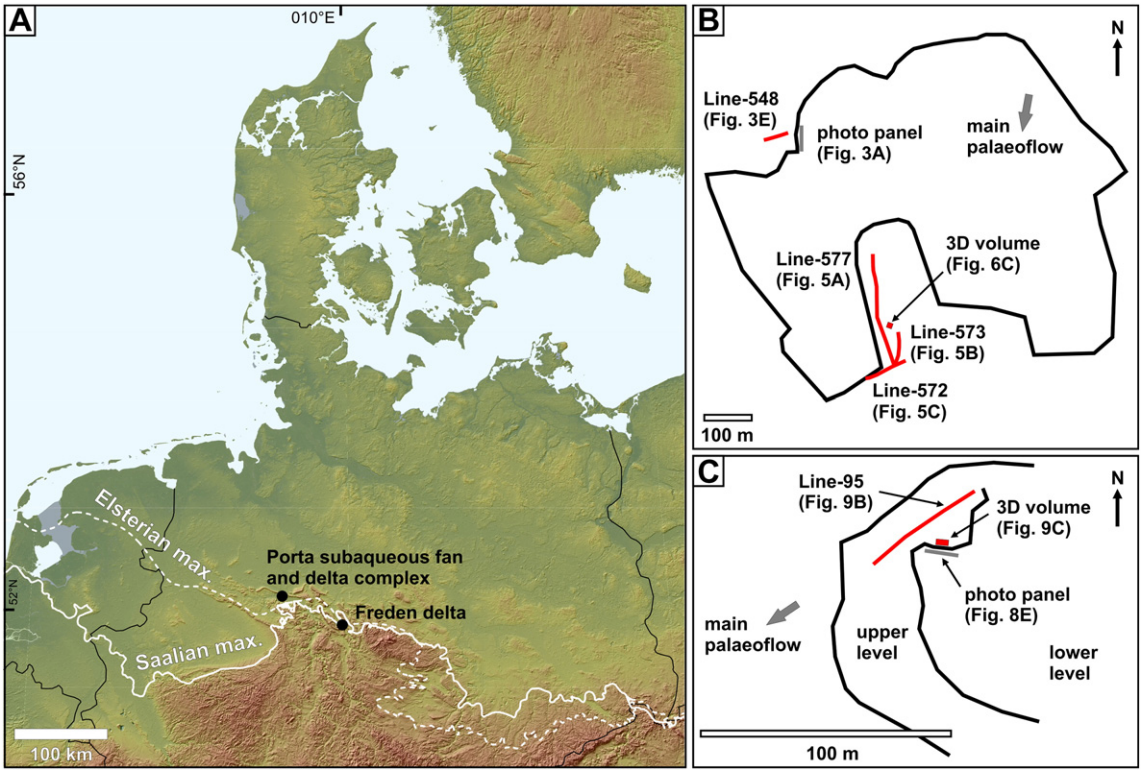

Fig. 1. (A) Overview map of the study area, showing the locations of the outcrops. The maximum extents of the Middle Pleistocene Elsterian and Saalian ice sheets are modified after Ehlers et al. (2011). The hill-shaded relief map was produced using Copernicus data and information funded by the European Union (EU-DEM layers). (B) Schematic map of the Porta site, showing the extent of the open-pit and the location of the GPR profiles and photo panel. (C) Schematic map of the Freden site, showing outcrop walls and the locations of the GPR profile and 3D volume.

pathways and the formation of extensive ice-dammed lakes (Eissmann 2002; Winsemann et al. 2007, 2009, 2011; Ehlers et al. 2011; Roskosch et al. 2015). Subaqueous ice-contact fans and glacifluvial deltas were deposited at the margins of these ice-dammed lakes and commonly include bedforms deposited by supercritical density flows (Hornung et al. 2007; Winsemann et al. 2009; Lang and Winsemann 2013).

The Porta subaqueous fan and delta complex has a radial shape with a maximum diameter of approximately 6.5 km and is up to 55 m thick (Hornung et al. 2007; Winsemann et al. 2009). The subaqueous ice-contact fan was deposited by sediment-laden meltwater jets, issuing from the ~600 m wide Porta Westfalica pass, which acted as a bedrock-feeder channel. It comprises three basal gravel-rich fan lobes, which spread radially from the bedrock feeder channel. These coarse-grained gravel lobes are onlapped and overlain by sand-rich fan lobes (Hornung et al. 2007; Winsemann et al. 2009). The studied gravel-rich central fan lobe is ~5500 m long, ~1000 m wide and 50 m thick. The sand-rich fan lobe is ~3000 m long, ~1200 m wide and 35 m thick, and onlaps and overlies the gravel-rich central fan lobe to the east. During a lake-level fall the subaqueous ice-contact fan was truncated and subsequently overlain by delta deposits. These delta deposits ("Porta delta") are up to 40 m thick and comprise two laterally stacked Gilbert-type deltas (Winsemann et al. 2009).

The glacifluvial Freden Gilbert-type delta is ~1 km wide, ~1.5 km long, up to 60 m thick and is located between two bedrock highs. The depositional architecture, which includes several vertically and laterally stacked delta lobes, indicates two genetically different delta bodies, which were deposited during two transgressive-regressive cycles (Winsemann et al. 2007; Roskosch et al. 2015). Within the delta body numerous shear-deformation bands occur, which probably represent coseismic features related to neotectonics (Brandes and Tanner 2012).

Previous studies of the Porta subaqueous fan and delta complex and the Freden delta have focussed on the overall depositional environments, the development of the large-scale depositional architecture during lake-level changes and numerical dating (Hornung et al. 2007; Winsemann et al. 2007, 2009, 2011; Roskosch et al. 2015). Sandy bedforms deposited by supercritical flows on the Porta subaqueous fan were analysed by Lang and Winsemann (2013). New outcrop sections in combination with GPR surveys provide new insights into the large-scale facies architecture and the three-dimensional geometry of both gravelly and sandy bedforms.

3. Methods

3.1. Facies analysis

The sedimentary facies were defined in the outcrops, noting grain size, bed thickness, bed contacts, bed geometry, internal sedimentary structures and soft-sediment deformation structures. Photos, 2D photo panels and line drawings document further details of the sedimentary facies and the facies architecture. The sedimentary facies are interpreted in terms of depositional processes (Table 1).

3.2. Ground-penetrating radar (GPR)

3.2.1. Acquisition of GPR profiles

In extensive surveys more than 10 km of GPR profiles were acquired. In this study, data from five selected GPR profiles with a total length of ~540 m are presented along with two high-resolution 3D GPR volumes. GSSI (Geophysical Survey Systems, Inc.) SIR-3000 (Surface Investigating Radar) and SIR-4000 GPR systems with 200 MHz, 400 MHz and 1.5 GHz shielded antennas were used for the acquisition of the GPR profiles. During the collection of the longer GPR profiles position and elevation were logged with a Trimble 5800 differential global positioning system (DGPS), yielding an accuracy in the centimetre ranges for lateral position and elevation. Radar trace distance, i.e., the distance between the shot points in profile direction, was 4 cm for the 2D profiles with the 200 MHz antenna. The high-resolution 3D grids were collected with 400 MHz and 1.5 GHz antennas. The 400 MHz data were collected with a distance of 5 cm between each parallel profile and the trace distance in profile direction was 2 cm. The 1.5 GHz data were collected with a profile distance of 2 cm and a trace distance of 0.4 cm. Data processing comprises time-zero correction, amplitude balancing by compensating spherical divergence and exponential attenuation, dewowing and bandpass filtering. The data were finally depth migrated by using a mean wave velocity and topographically corrected. The wave velocity was determined by diffraction-hyperbola analysis of the individual radar sections and varied between 0.075 and 0.11 m/ns, depending on the texture and water content of the sediment. The low-loss sandy and gravelly material enabled investigation depths of 1 to 6 m for the 1.5 GHz and 200 MHz antenna, respectively. The vertical resolution, i.e., the minimum distance between two interfaces needed to generate reflections that can be distinguished in the radargram, is approximately 4 cm for the 1.5 GHz antenna and 25 cm for the 200 MHz antenna. The horizontal resolution depends on the depth and ranges between 7 and 22 cm for the 1.5 GHz antenna (0.1–1 m depth) and 0.4 to 1.25 m for the 200 MHz antenna (0.5–5 m depth). Where possible, GPR sections were acquired next to outcrop walls to allow for a direct comparison between the GPR image and the outcrop section.

3.2.2. Interpretation of GPR data

Workflows for the sedimentological interpretation of GPR data have been proposed for example by Jol and Smith (1991), Gawthorpe et al. (1993), Bristow (1995) and Neal (2004), and are based on the principles of seismic facies analysis and seismic stratigraphy (Mitchum et al. 1977; Roksandic 1978; Sangree and Widmier 1979). Radar facies (RF) are defined based on the configuration, amplitude and continuity of the reflectors and their external geometries (Fig. 2). Bounding surfaces of radar facies and larger-scale architectural elements are defined by the terminations of the reflectors. For the description of the stacking pattern of architectural elements and element stacks the terminology of Pickering et al. (1995) was applied.

GPR has been successfully applied to various clastic depositional environments (Fielding et al. 1999; Bristow and Jol 2003; Bridge 2009; Andrews et al. 2016; Carling et al. 2016) and is able to resolve geometries on the scale of architectural elements and bedforms (Beres et al. 1995, 1999; Okazaki et al. 2013, 2015). For this study, facies architectures were mapped from 2D GPR profiles (200 and 400 MHz) beyond the scale of the available outcrop sections. Most sedimentary facies are well expressed by the corresponding radar facies in the GPR sections. Densely spaced grids of high-resolution GPR profiles (400 and 1500 MHz) were acquired to image the three-dimensional bedform architecture at selected sites. Although the acquisition and processing of high-resolution 3D GPR volumes is time consuming, the gained data are far more detailed and reliable and thus greatly enhance the reconstruction of the facies architectures (Beres et al. 1995; Grasmueck et al. 2004; Neal et al. 2008).

4. Results

4.1. Sedimentary facies and facies architecture of the Porta subaqueous ice-contact fan defined from outcrop sections

4.1.1. Gravel-rich subaqueous ice-contact fan deposits

The gravel-rich subaqueous ice-contact fan succession (Fig. 3) is characterised by (i) scours infilled by gravelly backsets (Gbl) (Fig. 3B), (ii) scours infilled by gravelly foresets (Gsc) (Fig. 3C), (iii) subhorizontally and low-angle cross-stratified gravel (Gl) (Fig. 3D), and (iv) trough cross-stratified gravel (Gt) (Table 1).

Large-scale amalgamated coarse-grained scour fills with gravelly foresets or backsets dominate the most proximal subaqueous fan deposits. Distally, scour fills become more isolated, finer-grained and commonly occur along laterally extensive erosional surfaces (Fig. 3A),

Table 1
Sedimentary facies observed in the studied outcrops.

Facies code	Description	Dimensions	Interpretation
Gravelly bedforms			
Gsc	Lenticular scours infilled by planar, trough or sigmoidal cross-stratified granule to cobble gravel. Thicker foresets occur within the larger scours and are characterised by coarse-tail normal grading perpendicular to the set boundaries. The clast fabric is aligned parallel to the foreset stratification with no preferred orientation of the clast axes.	Length: 1.1–25 m Thickness: 0.3–3 m Width: 2–8 m Foreset dip: 15–40°	Gravelly foresets represent the progradational infill of preformed scours (Carling and Glaister, 1987; Khadkikar 1999; Russell and Arnott 2003; Winsemann et al. 2009; Arnott and Al-Mufti 2017). Scouring is related to vortices generated by the expanding jet flow, hydraulic jumps or antidune-wave breaking (Long et al. 1991; Blair 1999; Russell and Arnott 2003; Cartigny et al. 2014).
Gbl	Lenticular scours infilled by backset cross-stratified granule to cobble gravel. Backsets have tangential basal contacts, are downflow divergent and commonly display normal distribution grading both perpendicular and tangential to the backset stratification. The clast fabric is upflow dipping with no preferred orientation of the clast axes and aligned parallel to the backset stratification.	Length: 1.7–4.6 m Thickness: 0.35–0.9 m Width: 2–13 m Backset dip: 12–44°	Scouring and deposition by isolated hydraulic jumps, probably representing chute-and-pool bedforms (Alexander et al. 2001; Fielding 2006; Lang and Winsemann 2013; Cartigny et al. 2014).
Gl	Tabular or lenticular beds of subhorizontally stratified and low-angle cross-stratified granule to cobble gravel. Beds commonly truncate each other at low angles. Internally, the beds display coarse-tail normal or inverse grading. The stratification style is variable, ranging from sharp-based spaced-stratified sets to crudely stratified sets with gradual basal contacts (sensu Hiscott 1994). Crudely stratified sets are characterised by grain-size variations, which define 0.15 to 0.3 m thick sets. The clast fabric is characterised by upflow imbrication with no preferred orientation of the clast axes.	Length:1.9–9.5 m (lenticular beds) Up to 15 m (tabular beds) Thickness: 0.2–1.5 m	Subhorizontally and low-angle cross-stratified gravel is interpreted as representing deposits of antidunes (Brennand 1994; Blair 2000; Russell and Arnott 2003; Duller et al. 2008; Lang and Winsemann 2013; Froude et al. 2017).
Gt	Trough cross-stratified granule to pebble gravel.	Length: 0.5–2.5 m Thickness: 0.3–0.8 m	Deposition by migrating 3D gravel dunes (Allen 1984; Khadkikar 1999).
Sandy bedforms			
Sbl	Lenticular scours infilled by backset cross-stratified sand, pebbly sand and gravel. Scours are mostly asymmetrical with a thicker downflow part. Some scour fills are massive, diffusely graded and may pass upslope into backset stratification. Gravelly scour fills display upslope dipping steep clast fabric with no preferred orientation of the clast axes. Backsets have concave-up, downflow divergent geometries and may display downflow transitions to convex-up or sigmoidal geometries. Farther downflow transitions into subhorizontally or sinusoidally stratified sand may occur. Flame structures and ball-and-pillow structures are observed within the scour fills and finer-grained substrata.	Length: 0.6–7 m Thickness: 0.08–1.6 m Width: 1–5 m Backset dip: 5–23°	Scouring and deposition by hydraulic jumps related to cyclic steps on the delta slopes (Postma and Cartigny 2014; Postma et al. 2014; Dietrich et al., 2016; Ventra et al. 2015).
Ssc	Lenticular scours infilled by backset cross-stratified sand to pebbly sand. Backsets are planar or concave-up and strongly downflow divergent. The margins of the scours may be very steep. Gravel lags are common at the base of the scours. Locally, massive or diffusely graded scour fills are observed. Scour fills commonly include decimetre-scale sandy intraclasts.	Length: 0.4–4 m Thickness: 0.08–1.2 m Width:0.5–2 m Backset dip: 10–20°	Scouring and deposition by isolated hydraulic jumps, probably representing chute-and-pool bedforms (Alexander et al. 2001; Fielding 2006; Lang and Winsemann 2013; Cartigny et al. 2014).
Sl	Tabular beds of subhorizontally stratified or low-angle cross-stratified pebbly sand. Cross-sets may dip both upflow and downflow. Internal erosional truncations are common. Locally, beds are draped by thin (0.5–1 cm) massive silty fine-grained sand layers.	Lateral extent: 0.5–16 m Thickness: 0.3–1.5 m Width: 0.5–4 m Dip: 5–15°	Deposition by breaking and upflow migrating antidunes (Alexander et al. 2001; Fielding 2006; Lang and Winsemann 2013; Cartigny et al. 2014).
Ss	Tabular beds of sinusoidally stratified pebbly sand. Laterally, the thickness pinches and swells slightly due to converging and diverging stratification. Internal low-angle truncations are common. Locally, beds are draped by thin (0.5–1 cm) massive silty fine-grained sand layers.	Lateral extent: 7–40 m Thickness: 0.5–1.2 m Width: 3–13 m Wavelength: 1.2–12 m	Deposition by quasi-stationary, aggrading antidunes (Allen 1984; Russell and Arnott 2003; Duller et al. 2008; Lang and Winsemann 2013).
Ssi	Tabular beds of sigmoidal stratified sand and pebbly sand, displaying differentiation into topset, foreset and bottomset laminae.	Lateral extent: 0.5–25 m Thickness: 0.1–2 m Width: 0.5–6 m Foreset dip: 15–35°	Deposition by humpback dunes (Saunderson and Lockett 1983; Fielding 2006; Lang and Winsemann 2013).
Sp/*St*	Planar or trough cross-stratified sand and pebbly sand.	Length: 0.3–8 m Thickness: 0.15–1.5 m	Deposition by migrating 2D or 3D dunes (Allen 1984; Winsemann et al. 2009).
Sr	Fine- to coarse-grained climbing ripple cross-laminated (silty) sand. Locally, upslope migrating climbing ripples occur.	Thickness: 0.1–0.7 m	Deposition from subcritical flows at high rates of suspension fall-out (Ashley et al. 1982; Allen 1984; Winsemann et al. 2007). Upslope migrating climbing ripples may relate to large-scale cyclic steps.
Fm	Massive silt and mud.	Thickness: 0.01–0.05 m	Deposition by suspension fall-out (Allen 1984).

which may be armoured by cobble to boulder lags. In the more proximal outcrops, scour fills are dominated by gravelly foresets, while in the more distal outcrops backsets and foresets are equally common. The dimension of the scours also decreases rapidly from proximal to distal. Above the erosional surfaces dm- to m-thick successions of laterally discontinuous subhorizontally stratified and low-angle cross-stratified

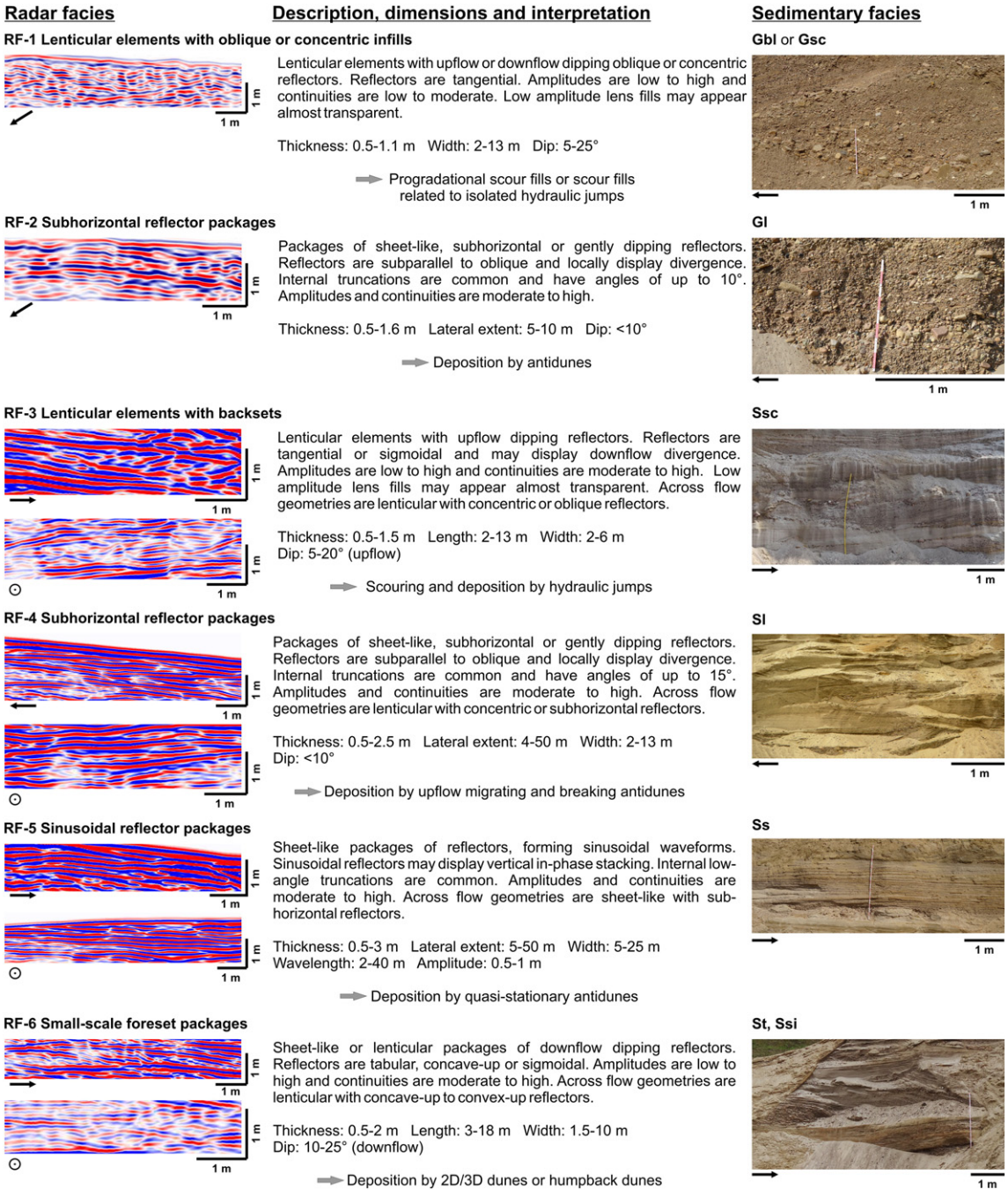

Fig. 2. Examples, description and interpretation of the characteristic radar facies of the subaqueous ice-contact fan successions (RF-1 to RF-6). The photos show the corresponding sedimentary facies.

gravel (Gl) occur (Fig. 3A). Locally, trough cross-stratified gravel (Gt) forms the uppermost part of these successions.

4.1.2. Sand-rich subaqueous ice-contact fan deposits

The sand-rich subaqueous ice-contact fan succession is characterised by (i) scours infilled by massive or diffusely graded or backset cross-stratified pebbly sand (Ssc) (Fig. 4A-D), (ii) subhorizontally stratified (Sl), low-angle cross-stratified (Sl) or sinusoidally stratified pebbly sand (Ss) (Fig. 4E-G), (iii) sigmoidally cross-stratified pebbly sand (Ssi) (Fig. 4H, I), (iv) planar or trough cross-stratified pebbly sand (Sp/*St*), and climbing-ripple cross-laminated sand (*Sr*) (Table 1).

Sheet-like beds of subhorizontally stratified (Sl), low-angle cross-stratified (Sl) or sinusoidally stratified pebbly sand (Ss) are interbedded with sigmoidally cross-stratified pebbly sand (Ssi) and form the characteristic facies association of the sand-rich fan deposits. Vertical and lateral facies transitions between these facies types are very common (Fig. 4H, I). Sigmoidally cross-stratification (Ssi) commonly flattens-out upwards and evolves into sinusoidally stratification (Ss). Locally, erosionally-based planar and trough cross-stratified pebbly sand (Sp/*St*) is intercalated. Downflow, the deposits pass into successions dominated by trough cross-stratified pebbly sand and climbing-ripple cross-laminated sand (*Sr*) (Hornung et al. 2007; Winsemann et al. 2009).

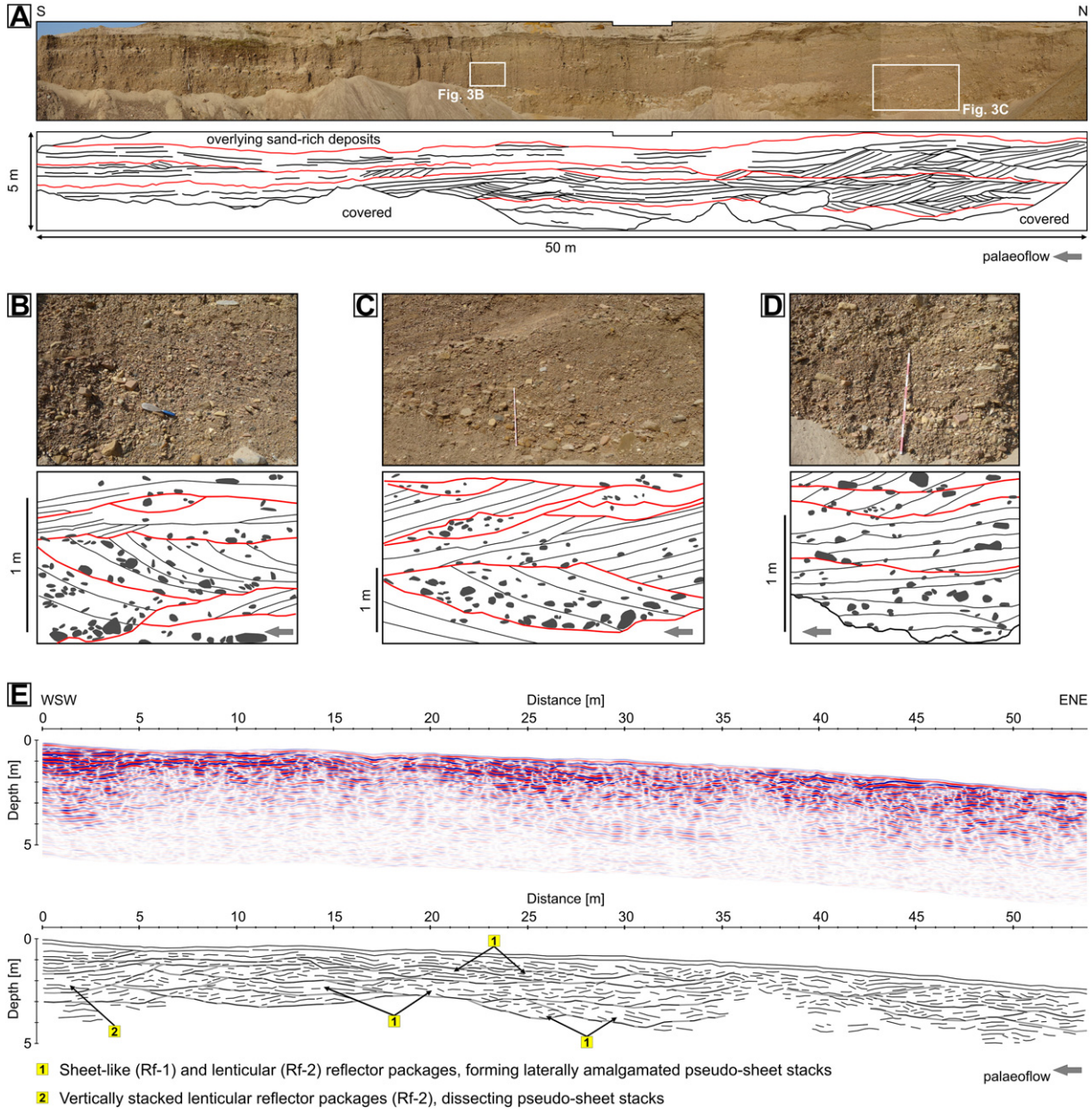

Fig. 3. Sedimentary facies and facies architecture of the gravel-rich subaqueous ice-contact fan deposits. (A) Interpreted photo panel from the distal gravel-rich deposits of the Porta subaqueous ice-contact fan. Location is given in Fig. 1B. (B) Close-up photo and line drawing of a scour fill with gravelly backsets (Gbl). The location of the photo is indicated in Fig. 3A. (C) Close-up photo and line drawing of gravelly scour fills with foresets (Gsc) and backsets (Gbl). The location of the photo is indicated in Fig. 3A. (D) Close-up photo and line drawing of subhorizontally stratified and low-angle cross-stratified gravel (Gl), overlain by trough cross-stratified gravel (Gt). The photo was taken next to the section shown in Fig. 3A. (E) GPR section (Line Porta-548, 200 MHz) of the distal gravel-rich subaqueous ice-contact fan deposits. The section is oriented oblique to the palaeoflow direction. Location is given in Fig. 1B.

4.2. GPR analysis of the Porta subaqueous ice-contact fan deposits

4.2.1. Gravel-rich fan deposits

The analysed GPR section has been acquired in the distal part of the gravel-rich succession and is oriented oblique to the palaeoflow direction (Fig. 3E). The facies architecture of the gravel-rich subaqueous fan deposits is characterised by lenticular and sheet-like reflector packages (Figs. 2, 3E). Lenticular reflector packages (RF-1) with upflow or downflow dipping oblique or concentric reflectors are 2 to 13 m wide. Sheet-like reflector packages (RF-2) are intercalated with the lenticular reflector packages (RF-1) and have lateral extents of 5 to 10 m. The contacts between the individual lenticular and sheet-like reflector packages are always erosional and the whole section is characterised by intense amalgamation. Within laterally more extensive and thicker sheet-like reflector packages smaller-scale lenticular reflector packages are locally embedded.

On a larger-scale, the lenticular (RF-1) and sheet-like (RF-2) reflector packages form laterally amalgamated pseudo-sheet stacks, which are ~1 m thick and have lateral extents of 20 to more than 50 m (Fig. 3E). Within the GPR-section three to four of these amalgamated pseudo-sheets are vertically stacked. Locally, vertically amalgamated stacks of lenticular reflector packages (RF-1), which are ~2 m thick and ~8 m wide, dissect the pseudo-sheets (Fig. 3E).

4.2.2. Sand-rich fan deposits

The facies architecture of the sand-rich subaqueous fan deposits is characterised by laterally extensive lenticular architectural elements, displaying sheet-like or mounded internal reflector patterns (Figs. 2, 5,

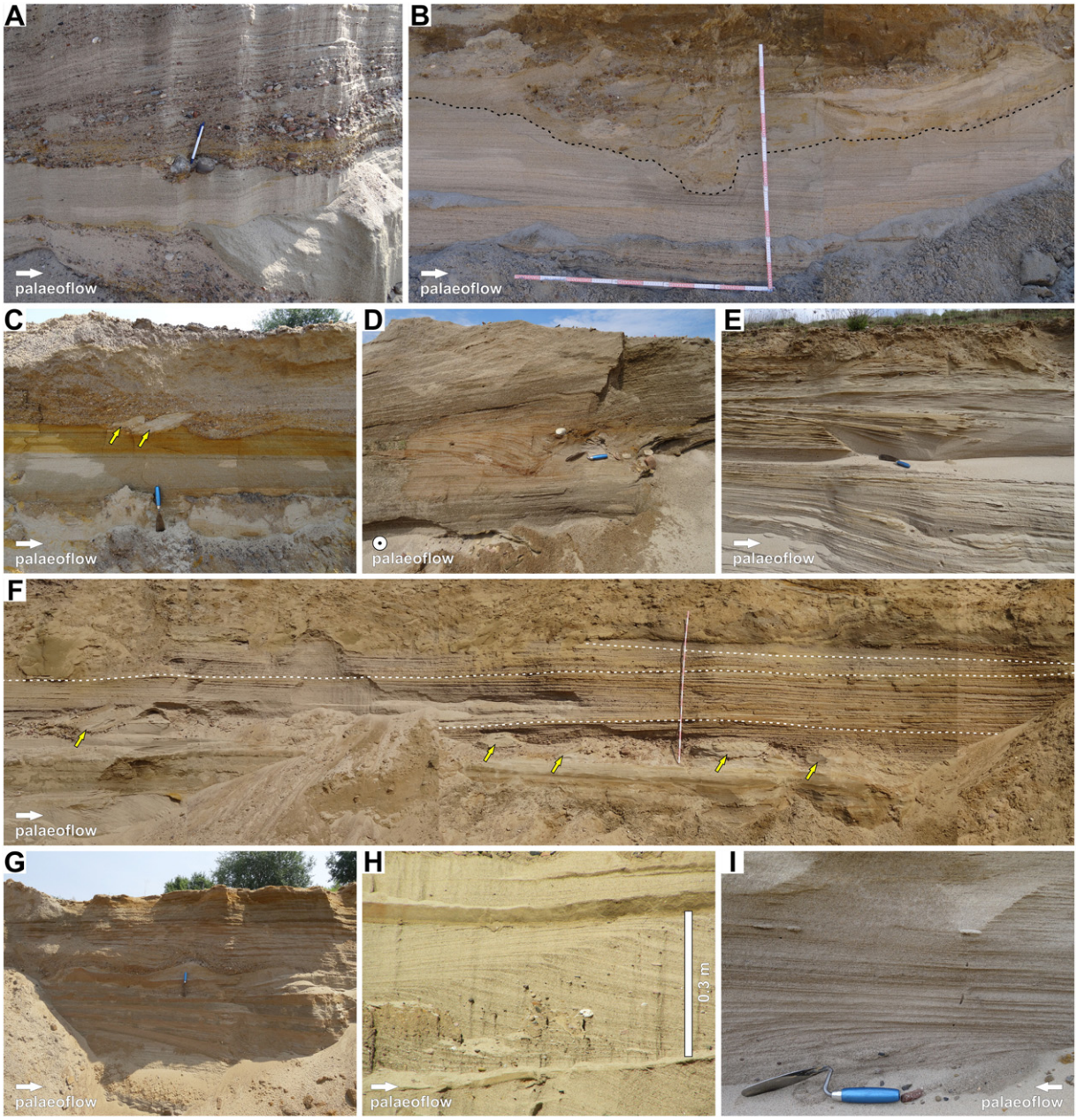

Fig. 4. Sedimentary facies of the sand-rich subaqueous ice-contact fan deposits. (A) Scooped scour base, overlain by gently dipping backsets deposited by a hydraulic jump (Ssc). Palaeoflow is from the left. Pen for scale is 12 cm long. (B) Massive to diffusely stratified sandy scour fill with steep-walled irregular base, indicating erosion and deposition in a hydraulic-jump zone (Ssc). Palaeoflow is from the left. (C) Irregular scour surface within antidune deposits (Sl, Ss) with large imbricated sandy intraclasts (arrows). Palaeoflow is from the left. Trowel for scale is 28 cm long. (D) Concentric scour fills (Ssc) within antidune deposits (Sl). Palaeoflow is towards the observer. Trowel for scale is 28 cm long. (E) Steep walled scour fill within antidune deposits (Sl). Palaeoflow is from the left. Trowel for scale is 28 cm long. (F) Sinusoidally stratified pebbly sand (Ss) deposited by quasi-stationary antidunes. Note the erosional base with sandy intraclasts (arrows) and the low-angle internal truncations (dashed lines). Palaeoflow is from the left. (G) High-relief erosional surface between sets of antidune deposits (Sl, Ss). Palaeoflow is from the left. Trowel for scale is 28 cm long. (H) Sigmoidally stratified pebbly sand (Ssi) deposited by humpback dunes. Palaeoflow is from the left. (I) Sigmoidally stratified pebbly sand (Ssi) deposited by humpback dunes, passing upwards into subhorizontally stratified sand (Sl) deposited by antidunes. Palaeoflow is from the right. Trowel for scale is 28 cm long.

6). The lenticular elements are 11 to 130 m long, 10 to 33 m wide and 0.75 to 2.5 m thick. The downflow and upflow margins of these elements are commonly truncated and may give them a rather wedge-shaped external geometry. Their bases are erosive and truncate reflectors from underlying deposits. Laterally, reflectors onlap onto the margins of the adjacent truncated lenticular elements. Internally, these elements are dominated by subhorizontal (RF-4) and sinusoidal (RF-5) reflectors, which are mostly base parallel. Across flow sections commonly display convex-up reflectors with downlapping contacts. Internal truncations are very common, especially between different radar facies. The sheet-like reflectors of RF-4 and RF-5 are associated with backset (RF-3) and foreset (RF-6) packages (Fig. 6A).

Although the internal architecture of the lenticular elements displays some variability, a characteristic pattern can be recognised (Fig. 6A). Backset packages (RF-3), infilling erosionally-based, flat-topped troughs, typically occur in the basal proximal part. Locally, the backsets display lateral transitions into convex-up or gently downflow dipping reflectors. More commonly, the backset packages pass laterally into subhorizontal reflectors of RF-4 or sinusoidal reflectors of RF-5. Packages of RF-4 and RF-5 represent the most extensive radar facies.

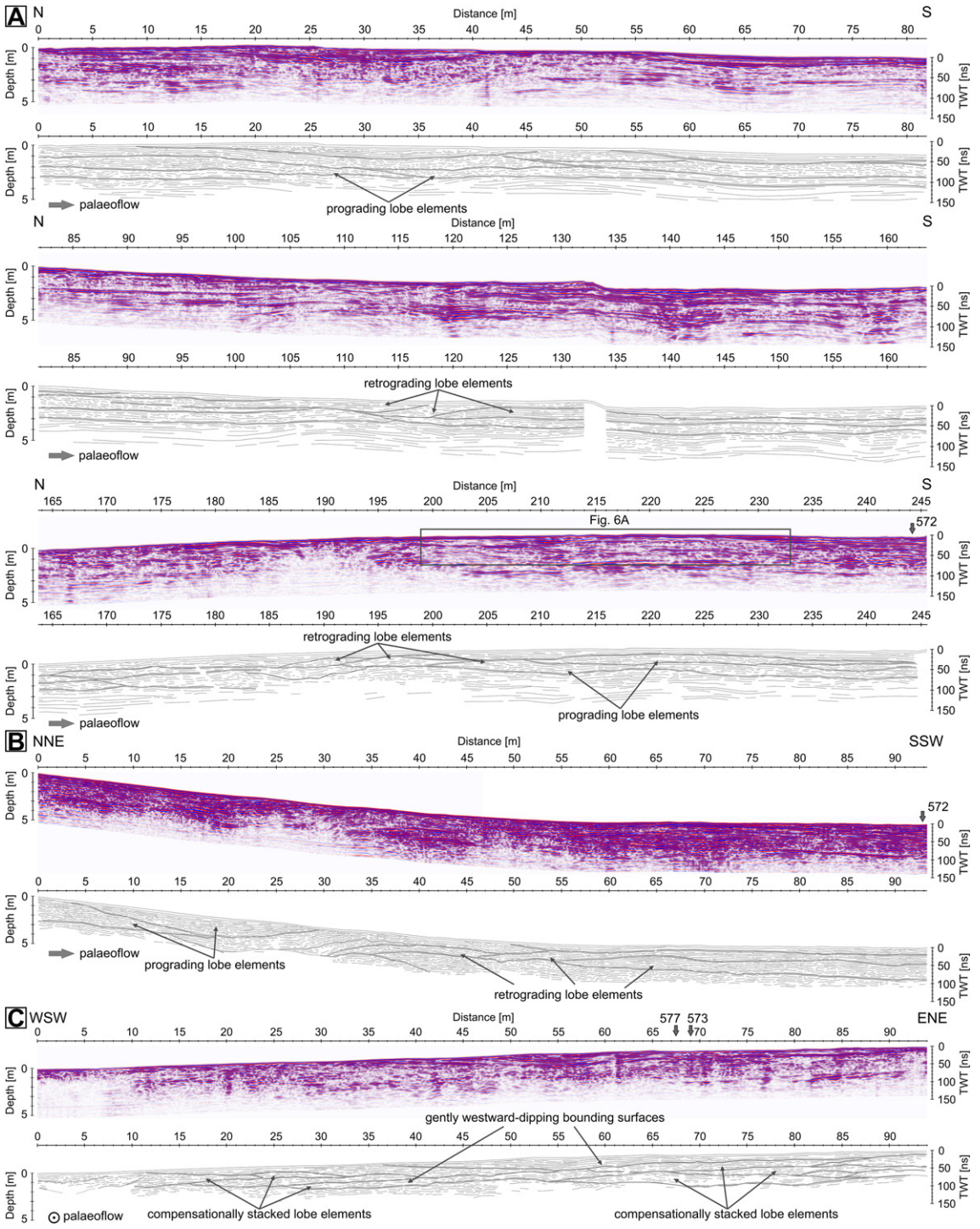

Fig. 5. Interpreted GPR sections of the sand-rich subaqueous ice-contact fan deposits. Locations are given in Fig. 1B. Grey arrows indicate intersections of the lines. (A) Line Porta-577 (200 MHz), measured slightly oblique to the palaeoflow direction. (B) Line Porta-573 (200 MHz), measured approximately parallel to the palaeoflow direction. (C) Line Porta-572 (200 MHz), measured approximately perpendicular to the palaeoflow direction.

Foreset packages of RF-6 are usually observed in the upper distal part. These foreset packages may truncate underlying reflectors of RF-4 and RF-5. Lateral transitions from subhorizontal reflectors of RF-4 into sigmoidal foresets of RF-6 are observed. Downflow flattening of sigmoidal foresets and transition into subhorizontal reflectors also occurs. Isolated backset or foreset packages with low extents are intercalated between subhorizontal and sinusoidal reflectors (Fig. 6A, C).

The larger-scale stacking pattern is characterised by laterally offset and compensational stacking. Stacks of laterally offset stacked lenticular elements consist of two to five individual elements and may display either progradational or retrogradational trends (Fig. 5A, B). Laterally stacked lenticular elements form vertical stacks, which are separated by laterally extensive erosive bounding surfaces, which can be traced across the whole length of the GPR sections. The bounding surfaces are subhorizontal or dip gently downflow. In the perpendicular to palaeoflow section compensational stacking is dominant. Laterally extensive bounding surfaces in this section dip gently towards westerly directions (Fig. 5C).

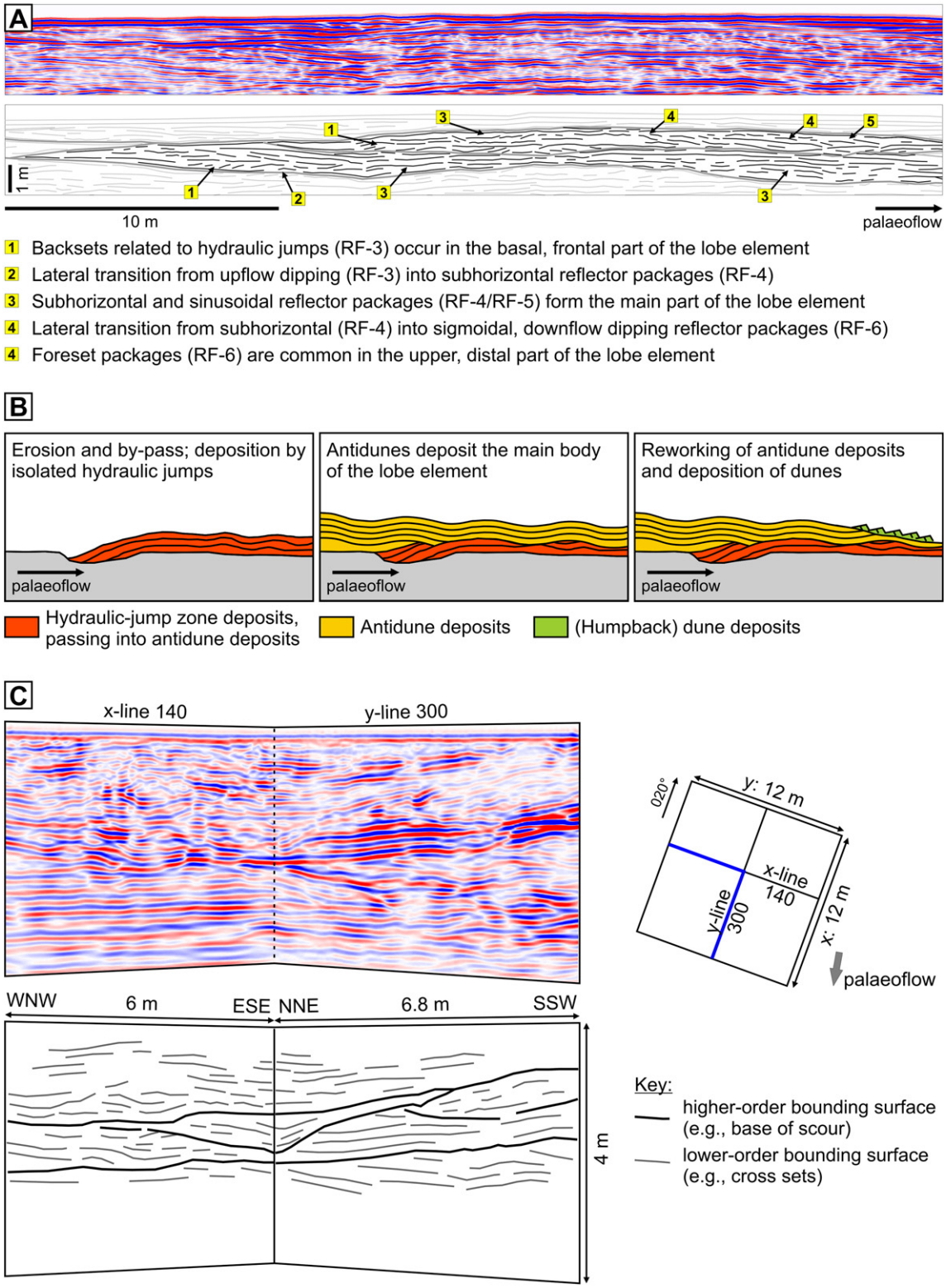

Fig. 6. (A) Close-up from GPR section Porta-577, showing two progradingly stacked lobe elements with their characteristic internal architectures. The location of the close-up view is given in Fig. 5A. (B) Schematic sketch of the depositional model for lobe elements. Sketch is not to scale. (C) Perspective view into the 3D GPR volume (400 MHz) acquired from the Porta subaqueous fan deposits, showing antidune deposits (RF-4) and scour fills related to hydraulic jumps (RF-3). The deposits are an analogue to the outcrop example in Fig. 4D.

4.3. Interpretation

4.3.1. Deposition of the gravel-rich subaqueous ice-contact fan succession

The facies architecture indicates that the deposition of the proximal part of the gravel-rich fan lobe was characterised by repeated scour-and-fill processes. Intense erosion and the formation of gravelly scour fills (Gsc) are attributed to the strong vortices generated by the expanding glacigenic jet flow, hydraulic jumps or antidune-wave breaking (Powell 1990; Long et al. 1991; Blair 1999; Russell and Arnott 2003; Cartigny et al. 2014; Froude et al. 2017). The observed rapid decrease in scour dimensions and grain size along the palaeoflow direction indicates waning flow conditions related to the expansion, deceleration

and the transformation of the glacigenic jet flow into a sustained density flow (Powell 1990; Russell and Arnott 2003; Winsemann et al. 2009). The occurrence of both backsets (Gbl) and foresets (Gsc) within the scour fills (Fig. 3) may be related to either different processes, which control the filling of the scours, or the highly variable geometry of bedforms related to supercritical flows. Progradational infilling of preformed scours (Gsc) occurs by flows with lesser sediment concentration, where a temporal lag between the souring and the infilling process occurs (Allen 1984; Arnott and Al-Mufti 2017). Alternatively, the foreset-dominated scour fills (Gsc) may indicate deposition downflow of a hydraulic jump, as it has been observed for experimental chutes-and-pools, which may produce downflow dipping cross-sets under very high aggradation rates (Cartigny et al. 2014). However, the dominance of foresets in the proximal scours probably points to progradational infilling of preformed scours and bypass of the eroded material to the more distal part of the gravel-rich fan lobe.

The facies architecture of the more distal part of the gravel-rich lobe is characterised by an association of deposits of large-scale scour fills, chutes-and-pools, antidunes and 3D gravel dunes, pointing to deposition by waning pulses of supercritical flows (Lang and Winsemann 2013; Cartigny et al. 2014). Scouring and the deposition of backsets are related to the early stage, highly supercritical flows. Gravel lags at the bases of the scours and along the erosional surfaces indicate reworking and the removal of all but the coarsest grain-sizes (Nemec et al. 1999; Winsemann et al. 2009). Subhorizontally and low-angle cross-stratified gravel (Gl) indicates deposition beneath more stable in-phase antidune waves (Brennand 1994; Breakspear 2008; Duller et al. 2008). Repeated steepening and eventually breaking of antidune waves trigger alternating phases of erosion and deposition and the formation of subhorizontal sets of coarser- and finer-grained gravel (Blair 1999, 2000; Duller et al. 2008). The threshold for antidune-wave breaking is lower above gravel beds than above sand beds due to the increased turbulence in flows over rougher beds (Breakspear 2008). The frequency and intensity of the erosional phases controls the occurrence of tabular or lenticular bed geometries within the gravelly antidune deposits (Gl) (Duller et al. 2008). Migrating gravel dunes indicate sustained high-energy subcritical flows (Allen 1984; Mulder and Alexander 2001; Carling 1999), which probably relate to the late stages of the flow events.

The analysed GPR section was measured oblique to the palaeoflow direction and indicates a predominance of lenticular geometries compared with the flow-parallel outcrop section (Fig. 3E). Previous observations from flume experiments and outcrops have shown that deposits of antidunes, which may display sheet-like geometries in flow-parallel sections, display lenticular across-flow geometries (Alexander et al. 2001; Yokokawa et al. 2010; Lang and Winsemann 2013; Froude et al. 2017). These lenticular geometries are related to 3D antidunes, which are generated by wave interferences in 2D antidunes and commonly form prior to antidune-wave breaking (Yokokawa et al. 2010).

The formation of pseudo-sheets by the amalgamated lenticular scour-fill, chute-and-pool and antidune deposits indicates lateral spreading of the flow during flow events, which was probably controlled by the topography created by the previously deposited bedforms. The vertical stacking of the amalgamated pseudo-sheets relates to the overall high rates of aggradation. Deposition by antidune trains with laterally changing local depocentres may indicate short-lived bores (Froude et al. 2017). The larger-scale aggrading pseudo-sheets (Fig. 3E) probably represent deposits of different flow events.

4.3.2. Deposition of the sand-rich subaqueous ice-contact fan succession

The sand-rich subaqueous fan succession is dominated by interbedded deposits of aggrading quasi-stationary antidunes (Ss) and humpback dunes (Ssi), which are characteristic bedforms of supercritical to transcritical flows The stationary antidune deposits represent phases of sustained quasi-steady flows and are separated by deposits of either higher-energy supercritical flows (chutes-and-pools and breaking antidunes), or lower-energy subcritical flows (humpback dunes, 3D dunes and climbing ripples, cf., Lang and Winsemann 2013).

The larger-scale facies architecture of the sand-rich fan succession is imaged in the GPR sections and is characterised by lenticular elements, which build the larger-scale sand-rich fan deposits (Figs. 5, 6). Based on their external and internal geometries these architectural elements are interpreted as representing lobe elements (cf., Mutti and Normark 1987; Gervais et al. 2006; Deptuck et al. 2008; Prelat et al. 2010). Erosional basal contacts are very common in proximal lobe deposits (Gervais et al. 2006). Laterally more extensive erosional surfaces indicate bypass of sediment probably related to phases of fan progradation or larger flow events. The internal architecture of the lobe elements displays recurrent lateral and vertical successions (Fig. 6A, B), which are characterised by (i) scouring and deposition related to hydraulic jumps in their basal, proximal parts, (ii) deposits of antidunes that form their main bodies and (iii) deposits of (humpback) dunes in their upper, distal parts. The recurrent facies architecture suggests that the lobe elements represent supercritical morphodynamic successions (sensu Demko et al. 2014) related to the spatio-temporal evolution of the formative flow. Supercritical morphodynamic successions are characterised by a scoured basal surface, overlain by massive, crudely stratified or backset cross-stratified hydraulic-jump deposits that pass upwards into deposits of antidunes, followed by deposits of dunes and ripples (Demko et al. 2014). Such supercritical morphodynamic successions were described from the channel-lobe transition zones of coarse-grained submarine fan deposits (Demko et al. 2014; Postma et al. 2015). Basal erosion and the occurrence of backsets indicate hydraulic-jump formation in the initial flow stage, when the highest Froude number occur and flows become unstable (Cartigny et al. 2014). Additional field evidence for hydraulic jumps is provided by the very steep-walled scour margins and the preservation of large friable sandy intraclasts (Leclair and Arnott 2003; Postma et al. 2009, 2014; Winsemann et al. 2009) (Fig. 4B, C). Backsets form trains that can laterally be traced for ~10 m (Fig. 6A), indicating upflow retreat of the hydraulic jump as known from cyclic steps (Postma et al. 2014; Ventra et al. 2015). The backset cross-stratified scour fills observed in the GPR sections (RF-3) are laterally commonly more extensive than the corresponding sedimentary facies (Ssc) mapped from discontinuous outcrop sections. The isolated scour fills (Ssc) are interpreted as deposits of isolated hydraulic jumps or chutes-and-pools (Lang and Winsemann 2013), which are formed by irregularly spaced, step-wise migrating hydraulic jumps (Fielding 2006; Cartigny et al. 2014). The GPR sections indicate that the laterally more extensive scour fills represent constituents of the lobe elements (Fig. 6A) and probably indicate hydraulic jumps in areas of flow choking at the stoss sides of the lobe elements (cf., Hamilton et al. 2015). Deposits of antidunes are the most extensive facies within the lobe elements (Figs. 5, 6A). Thick aggrading antidune deposits indicate stable, quasi-steady supercritical flows (Cheel 1990; Duller et al. 2008; Cartigny et al. 2014). This re-establishment of supercritical flows may relate to flow acceleration and thinning downflow of a hydraulic-jump zone compatible to the processes on the stoss sides of cyclic steps (Zhong et al. 2015; Lang et al. 2017). Alternatively, antidune formation may relate to wave trains formed downflow of an undular hydraulic jump (Broome and Komar 1979; Chanson 2001; Lang and Winsemann 2013). Deposition by dunes and humpback dunes in the upper, distal parts of the lobe elements indicate sustained subcritical flows that prevailed during a late stage of lobe-element deposition (Fig. 6B) (Allen 1984; Mulder and Alexander 2001). Small-scale facies changes within individual lobe elements point to short lived fluctuations of the flow conditions (Lang and Winsemann 2013).

Lobe elements and lobe-element stacks display as well aggrading, prograding, retrograding (Fig. 5A, B) as compensational stacking patterns (Fig. 5C). The variable stacking pattern of the lobe elements is common within lobe deposits and may reflect the impact of a variety

of internal (e.g., flow parameters, flow frequency, subtle topographic changes) and external (e.g., basin slope, base level, confinement) controlling factors (Gervais et al. 2006; Deptuck et al. 2008; Prelat et al. 2010; Hamilton et al. 2017). Gervais et al. (2006) presented a model for the autogenic generation of retrograding and prograding stacking pattern of lobe elements based on high-resolution seismic data from the Golo fan off Corsica. The relief created by previous deposits acts as frontal obstacle to the flow and forms a retrograding deposit upflow of the obstacle. Flow over the obstacle is accumulative and sediment is eroded and bypassed to the downflow end of the obstacle, where deposition resumes and a prograding lobe element is formed (Gervais et al. 2006). Flume-tank experiments by Hamilton et al. (2015, 2017) have refined this model and have shown that the depositional architecture of lobes and lobe-elements may relate to autogenic avulsion cycles of fan systems dominated by supercritical density flows. Lobe-element construction in such settings is characterised by an early prograding phase during channel extension and frontal-splay deposition and a later retrograding phase due to flow choking, resulting in hydraulic-jump formation and upslope retreat (Hamilton et al. 2015, 2017). The vertical stacking of lobe-element stacks points to highly aggrading conditions. The compensational stacking of lobe elements observed in the across flow section is a characteristic feature of lobe deposits and relates to the infilling of the topography between the individual lobe elements during lobe construction (Mutti and Normark 1987; Deptuck et al. 2008; Prelat et al. 2010).

4.4. Sedimentary facies and facies architecture of glacifluvial Gilbert-type delta deposits defined from outcrop sections

4.4.1. Porta delta

Delta-foreset deposits of the Porta Delta (Fig. 7) comprise medium- to very thick-bedded sand, pebbly sand and gravel, and have dips of 6–31°. Foreset beds are organised into 0.9 to 1.5 m thick fining-upward successions. Basal lenticular scours have scooped basal erosional surfaces and are filled by backset cross-stratified pebbly sand and gravel (Sbl) (Fig. 7A-D). The gravelly scour fills commonly display an upslope dipping steep-clast fabric with no preferred orientation of the clast axes and fine upslope (Fig. 7C). Sandy scour fills may have a massive, diffusely graded or deformed (convolute bedding and clastic dykes) basal part, passing upslope into backset cross-stratification (Fig. 7A, B). The scour fills are overlain by thin- to medium-bedded of low-angle cross-stratified or sinusoidally cross-stratified sand and pebbly sand (Sl, Ss). The sheet-like beds commonly have erosional basal contacts and display frequent internal truncations and small-scale concave-up scours, but lateral transitions from the scour fills into the sheet-like beds are also observed. Locally, beds are draped by thin massive silty fine-grained sand layers (Fig. 7E). Upwards, the thickness of bedsets commonly increases and sigmoidally cross-stratified pebbly sand occurs (Ssi). The tops of the fining-upward successions are formed by thin beds of climbing-ripple cross-laminated silty sand or massive silt and mud.

4.4.2. Freden delta

Delta-foreset deposits of the Freden delta comprise medium- to very thick-bedded sand and pebbly sand, and have dips of 5–34°. Laterally, a fining from coarser-grained foreset packages to finer-grained foreset packages is commonly observed.

Foreset beds consist of laterally extensive trains of regularly spaced scour fills with asymmetrical geometries (Fig. 8). Scours are filled by backset cross-stratified pebbly sand (Sbl). Backsets have concave-up, downflow divergent geometries and may display downflow transitions to convex-up or sigmoidal geometries (Fig. 8A, E). Perpendicular and oblique to the palaeoflow direction these deposits appear as troughs, which are filled with concentric to low-angle cross-stratified pebbly sand (Fig. 8B). Backsets may display downflow transitions into sheet-like low-angle cross-stratified (Sl) or sinusoidally stratified pebbly sand (Ss) (Fig. 8A). Locally, foreset beds consist entirely of medium- to thick-bedded low-angle cross-stratified (Sl) or sinusoidally stratified pebbly sand (Ss) (Fig. 8E).

Finer-grained sandy foreset beds commonly comprise planar or trough cross-stratified sand and pebbly sand (Sp/*St*). In the delta-toe zone of these foreset packages sigmoidal cross-stratified sand and

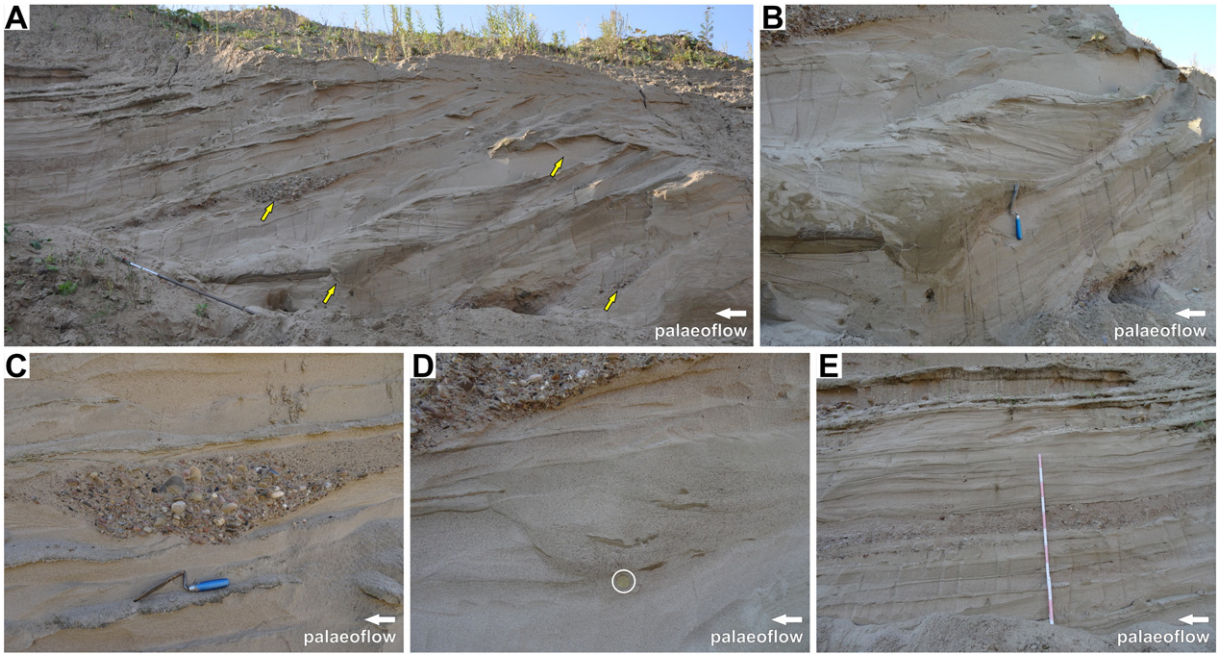

Fig. 7. Sedimentary facies and facies architecture of the Porta delta. (A) Delta foresets with isolated gravelly and sandy scour fills (arrows) related to cyclic steps (Sbl). Palaeoflow is from the right. Pick for scale is 164 cm long. (B) Delta foreset with sandy cyclic-step deposits (Sbl). The lower part of the scour fill is massive and deformed, passing upwards into backsets. Palaeoflow is from the right. Trowel for scale is 28 cm long. (C) Gravelly scour fill related to cyclic steps within delta foreset. Palaeoflow is from the right. Trowel for scale is 28 cm long. (D) Small-scale scour related to cyclic-steps within delta foreset. Mud clasts are incorporated into the scour fill. Palaeoflow is from the right. Coin for scale is 24 mm (circled). (E) Sandy antidune deposits (Ss, Sl) within delta foreset. Palaeoflow is from the right.

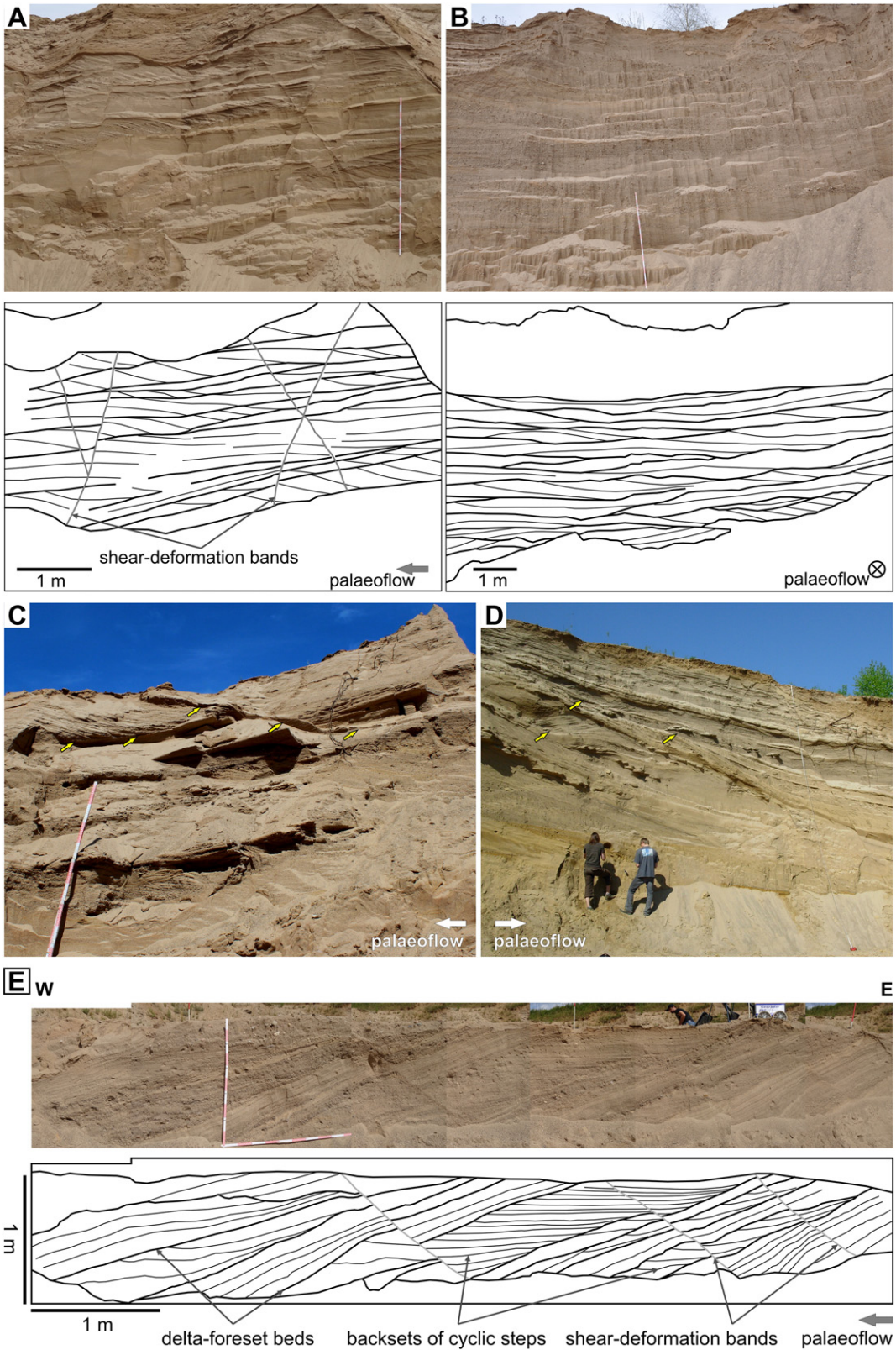

Fig. 8. Sedimentary facies and facies architecture of the Freden delta. (A, B) Photos and line drawings of delta foreset with cyclic-step deposits (Sbl). The outcrop sections are ~10 m apart. (A) Outcrop section parallel to the palaeoflow direction. (B) Outcrop section perpendicular to the palaeoflow direction. (C) Internal truncations (arrows) by regularly spaced scours within cyclic-step deposits (Sbl). Palaeoflow is from the right (Photo by courtesy of C. v. Wolff). (D) Isolated backset cross-stratified scour-fills (arrows) related to cyclic steps (Sbl) within foreset packages dominated by climbing-ripple cross-laminated sand. Palaeoflow is from the left (Photo by courtesy of C. Brandes). (E) Interpreted photo panel taken next to the 3D GPR volume (Fig. 9C), showing delta foresets with backsets of cyclic steps.

pebbly sand (Ssi) is common. Foreset packages dominated by thick-bedded climbing-ripple cross-laminated deposits consist of silty fine- to medium-grained sand (*Sr*). These ripple bedforms partly climb upslope. Locally, large isolated scours occur, which are filled with massive and backset cross-stratified pebbly sand (Sbl) and are typically deeper and larger than those in the coarser-grained foreset packages (Fig. 8D).

4.5. GPR analysis of the Freden delta

GPR sections are only available from the deposits of the Freden delta. The facies architecture of the Freden delta is characterised by large-scale delta-foreset beds of RF-7, consisting of laterally extensive, moderately to steeply dipping (5–25°), moderate to high amplitude reflector packages (Fig. 9). The total thickness of the foreset packages ranges from 10 to 25 m (Fig. 9A, B). Perpendicular to the palaeoflow, foreset packages form 15 to 70 m wide and 3 to 20 m thick laterally and vertically stacked mounds (Fig. 9A, C).

In flow direction, delta foreset beds commonly display regularly spaced lenticular scours, which represent deposits of cyclic steps (Fig. 9). These scours are 2 to 6 m long, 0.15 to 0.7 m deep and are characterised by tabular, concave-up or sigmoidal upslope-dipping reflectors with low to moderate amplitudes (RF-8). Along the delta foreset these lenticular scours form trains, which can be laterally traced for up to 15 m (Fig. 9B). Perpendicular to the palaeoflow, scours are 1 to 5 m wide and typically display concentric infills (Fig. 9C).

Downslope, the dip of the foreset beds decrease to less than 10° and a change to concave-up and convex-up geometries may occur, indicating the transition into toeset or bottomset deposits. Locally, backset trains or isolated scour fills with backsets (RF-8) can be observed, which have lower amplitudes and continuities, contrasting markedly with the surrounding foreset packages.

4.6. Interpretation

Bedforms observed in the glacifluvial deltas include deposits of cyclic steps (Sbl), antidunes (Sl, Ss), humpback dunes (Ssi), dunes (*St*) and climbing ripples (*Sr*) (Table 1; Figs. 7, 8, 9). Steep walled scours with scooped bases and massive, diffusely graded or backset cross-stratified infills (Sbl) indicate cut-and-fill processes related to hydraulic jumps (Cartigny et al. 2014; Postma and Cartigny 2014; Postma et al. 2014). The formation of dewatering structures in some scours indicates rapid suspension settling and pressure fluctuations in hydraulic-jump zones (Leclair and Arnott 2003; Postma et al. 2014). The regular spacing of the scours, which form laterally extensive trains along the delta-foreset beds, clearly points to deposition by upslope migrating cyclic steps (Cartigny et al. 2014; Ventra et al. 2015; Dietrich et al. 2016). Lateral transitions from the scour fills into antidune deposits (Sl, Ss) indicate the re-establishment of supercritical flow conditions on the stoss-sides of cyclic steps (Zhong et al. 2015; Lang et al. 2017). The occurrence of more extensive antidune deposits in some foreset beds points to temporarily lower Froude numbers within the supercritical density flows (Ventra et al. 2015). Scouring within the antidune deposits may relate to antidune-wave breaking (Lang and Winsemann 2013; Cartigny et al. 2014). The predominance of deposits of cyclic steps and antidunes within the delta-foreset succession indicates deposition by supercritical density flows (Postma and Cartigny 2014; Postma et al. 2014; Ventra et al. 2015; Lang et al. 2017).

4.6.1. Deposition of the Porta delta

Scour fills related to upslope migrating cyclic steps in the foreset deposits of the Porta delta are commonly isolated and widely spaced (Fig. 7A). The occurrence of more isolated cyclic-step deposits associated with antidune deposits may indicate deposition from waning surge-type supercritical density flows (Mulder and Alexander 2001), probably at the lower limit of the cyclic-step stability field (Lang et al. 2017). Alternatively, more isolated hydraulic-jump deposits may reflect rapidly decelerating and expanding low-efficiency flows, or short delta slopes, which prevent the re-establishment of supercritical flow conditions (Massari, 2017).

Further indicators for surge-type density flows are the small-scale fining-upward successions of cyclic-step (Sbl) and antidune deposits (Sl, Ss), which were probably triggered by frequent small-volume gravitational collapses of the upper delta slope (cf., Talling 2014) during high rates of delta-front aggradation (cf., Gobo et al. 2014, 2015). Drapes of silty fine-grained sand may indicate phases of deposition by suspension fall-out between the individual surges.

4.6.2. Deposition of the Freden delta

At the Freden delta (Fig. 8), deposits of cyclic steps can often be laterally traced along the entire length of the foreset beds and display little variation in thickness and grain size, indicating deposition by sustained supercritical density flows (Ventra et al. 2015). Thick deposits of (humpback) dunes and climbing ripples in the finer-grained foreset beds are further indicators for sustained density flows (Plink-Björklund and Steel 2004; Winsemann et al. 2007; Ghienne et al. 2010; Carvalho and Vesely 2017). In the delta toeset the deposition of humpback dunes and climbing ripples indicates highly aggradational conditions and sustained flows, probably related to a hydraulic jump at the basal break of slope (Winsemann et al. 2011; Jobe et al. 2012; Macdonald et al. 2013). Isolated backset cross-stratified coarse-grained scour fills in fine-grained delta-foreset beds, dominated by climbing-ripple cross-laminated sand and silt, record higher flow conditions probably related to major meltwater discharge events (e.g., Ghienne et al. 2010; Ventra et al. 2015; Carvalho and Vesely 2017) or major slope-failure events (Talling 2014; Hughes Clarke 2016). The upslope migrating climbing ripples have previously been interpreted as indicating backflows related to hydraulic jumps at the base of slope (Clemmensen and Houmark-Nielsen 1981; Winsemann et al. 2007). Alternatively, these upslope migrating climbing ripples may be related to the hydraulic-jump zone of large-scale cyclic steps. However, the outcrop conditions do not allow for an unambiguous interpretation.

5. Discussion

5.1. Deposition by supercritical density flows in subaqueous ice-contact fan settings

Subaqueous ice-contact fans represent an ideal example of jet-flow deposits, where the system does not evolve any further than the early jet-flow stage (Powell 1990; Hoyal et al. 2003; Russell and Arnott 2003) (Fig. 10A). The flow expands from a fixed conduit and the flow conditions in the conduit control the evolution of the depositional system. The deposition of the coarse-grained gravel-rich and sand-rich successions indicates high-discharge, sediment-laden flows, probably related to the drainage of subglacial or englacial reservoirs (Russell and Arnott 2003; Winsemann et al. 2009; Dowdeswell et al. 2015). Mäkinen (2003) described depositional sequences (metres to tens of metres thick) from esker-ice-contact fan successions, which include proximal gravel-rich deposits, passing downflow into sand-rich deposits, and interpreted them as annual sequences deposited by seasonal variations of meltwater discharge.

Subaqueous ice-contact fans display both similarities and differences to submarine fan settings, regarding bedforms and facies architecture. In submarine settings, deposits of supercritical density flows are generally associated with coarse-grained fan systems (Hoyal et al. 2011, 2014; Hamilton et al. 2015), which commonly occur on steep active continental margins (Mutti and Normark 1987; Pickering and Hiscott 2015; Lang et al. 2017). In contrast, the studied subaqueous ice-contact fan was deposited by a supercritical jet flow on a relatively flat basin floor (Winsemann et al. 2009; Lang and Winsemann 2013). The gravel-rich fan deposits are characterised by scour fills, chute-

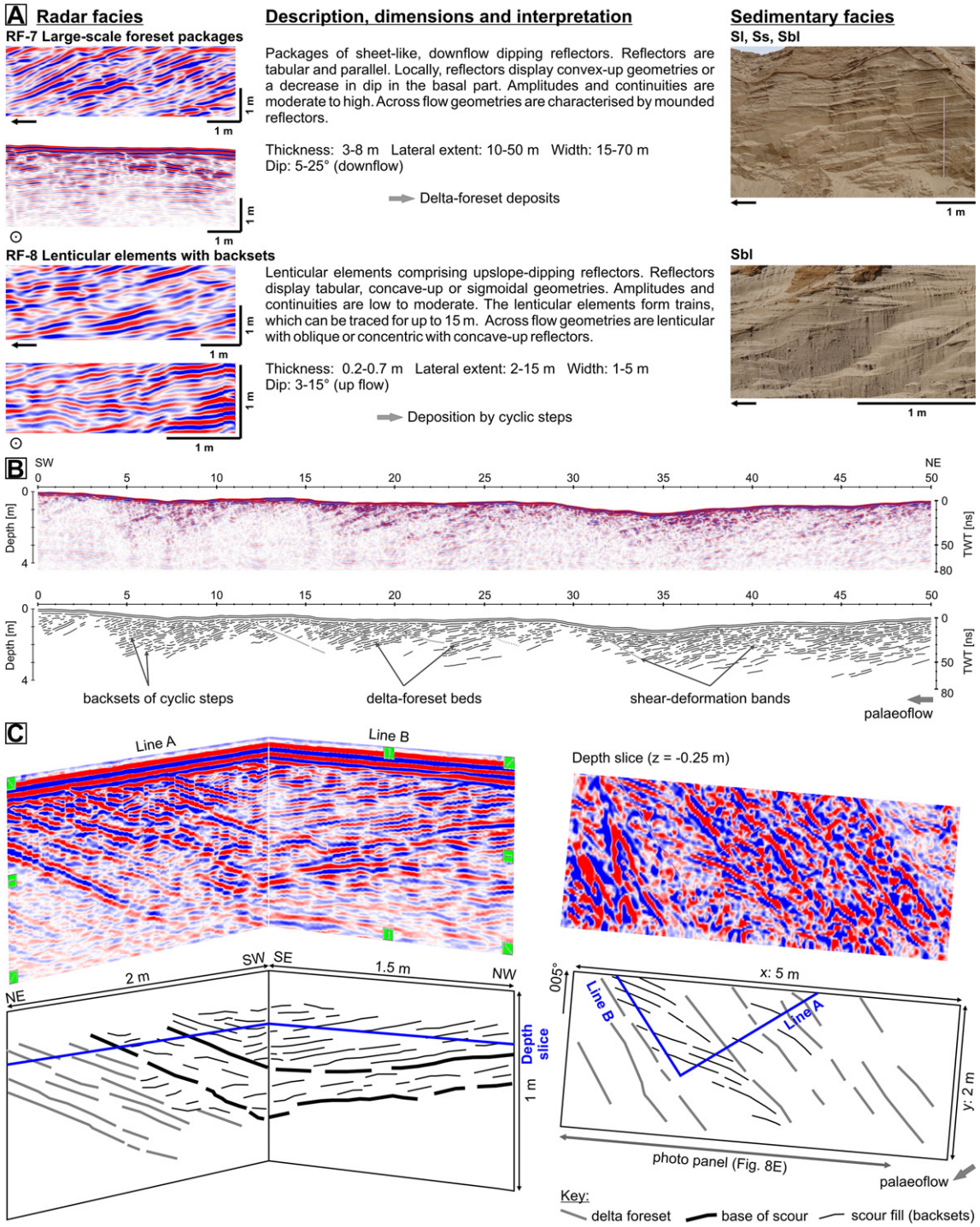

Fig. 9. (A) Examples, description and interpretation of the characteristic radar facies of the delta successions (RF-7 and RF-8). The photos show the corresponding sedimentary facies. (B) Interpreted GPR section (Freden-95; 400 MHz) from the delta deposits at Freden. Location is given in Fig. 1C. (C) Architecture of cyclic-step deposits, shown as a perspective view into the 3D GPR volume (1500 MHz) and as depth slice. Lines A and B are arbitrary lines oriented parallel (Line A) and perpendicular (Line B) to the palaeoflow direction.

and-pool and antidune deposits (Fig. 3), which indicate aggradational conditions despite their highly scoured nature. Unfortunately, the larger-scale facies architecture of the gravel-rich succession is beyond the scale of the acquired GPR sections. The deposits resemble those of coarse-grained, highly scoured channel-lobe transition zones of some turbidite systems (Wynn et al. 2002; Ito et al. 2014; Postma et al. 2015), which also represent regions of rapid flow expansion and deceleration (Hoyal et al. 2003; Van Wagoner et al. 2003). The aggrading stacking of the ice-contact fan deposits is probably related to the limited mobility of glacigenic jet flows. In supercritical turbidite systems the location of the channel-lobe transition zone is relatively mobile both laterally and along the slope profile (Hamilton et al. 2015, 2017). In contrast, glacigenic jet flows are limited to radial migration (Hoyal et al. 2003). Flow splitting occurs in response to sedimentation in front of the conduit and leads to radial spreading of the initial deposit, finally resulting in a rise of the depositional surface and aggradation (Van Wagoner et al. 2003; Winsemann et al. 2009). The sand-rich fan deposits probably represent a stage, where the glacigenic jet flow has already evolved into a sustained density flow on the lee side of the mouth bar (Fig. 10A). Mapping of the large-scale facies architecture

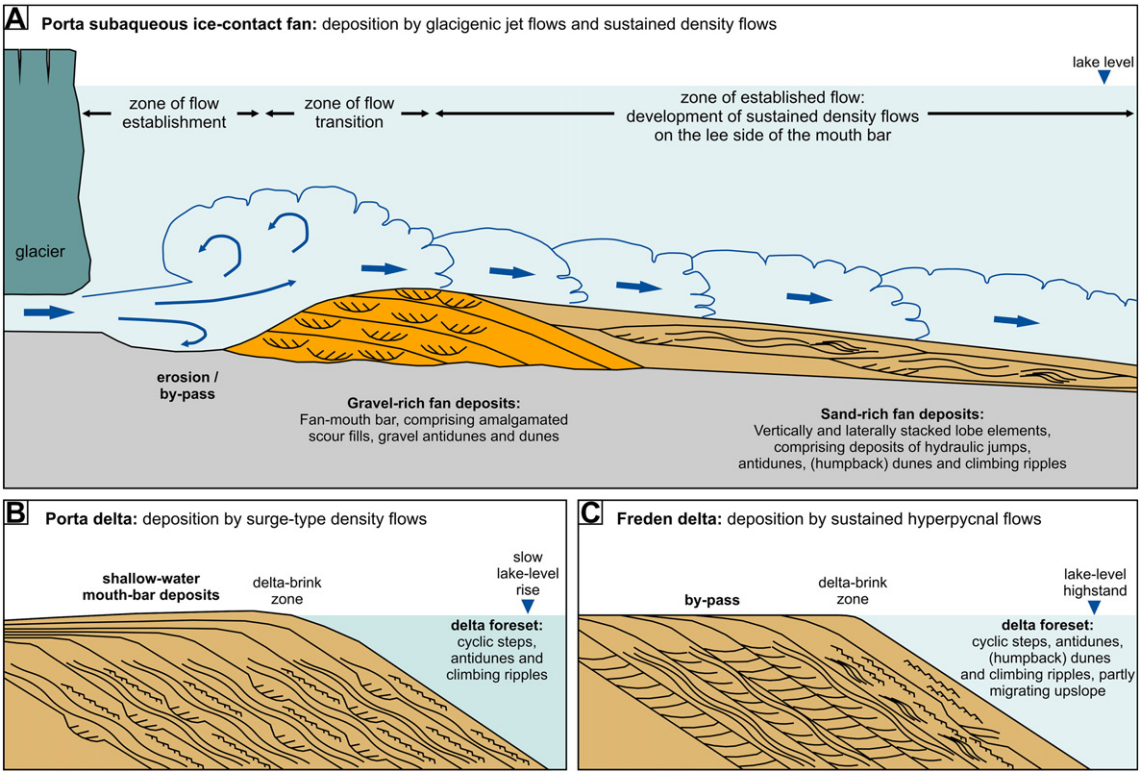

Fig. 10. Schematic sketches to illustrate the depositional models. Sketches are not to scale. (A) Depositional model for gravel-rich and sand-rich subaqueous ice-contact fans deposited by glacigenic jet flows (partly adapted from Lang and Winsemann 2013; Dowdeswell et al. 2015). (B) Depositional model for the glacifluvial Porta delta. Foreset beds are mainly deposited by surge-type supercritical density flows. (C) Depositional model for the glacifluvial Freden delta. Foreset beds are mainly deposited by sustained supercritical density flows (B and C are partly adapted from Gobo et al. 2014).

and stacking pattern of the sand-rich lobe elements from the GPR sections reveals a high degree of similarity to sand-rich lobe deposits of submarine fans (Gervais et al. 2006; Deptuck et al. 2008; Hamilton et al. 2017) (Fig. 5). Prograding and retrograding stacking of lobe elements relates to the interaction of the flow with the basal topography (cf., Gervais et al. 2006) and autogenic avulsion processes in a feeder system dominated by supercritical density flows (Hamilton et al. 2015, 2017). The sand-rich lobe elements are interpreted as small-scale lateral and vertical successions related to individual flow events and their interaction with the bed topography. An ideal succession consists of a basal erosional surface overlain by hydraulic-jump related backsets, which pass upwards and downflow into antidune deposits and further into deposits of (humpback) dunes (Fig. 6A, B). Similar supercritical morphodynamic successions were described from deposits of the channel-lobe transition zone related to supercritical density flows (Demko et al. 2014; Postma et al. 2015).

Antidune deposits represent characteristic facies of the sand-rich subaqueous ice-contact fan deposits, forming the main body of the lobe elements, and are a common feature of turbidity flow deposits in submarine fans (Hand 1974; Ito and Saito 2006; Ito 2010; Lang et al. 2017). They probably represent typical features of unconfined fan regions, where flow expansion lowers the flow competence and Froude numbers, while aggradation rates increase (Fedele et al. 2017). In contrast, cyclic-step deposits are ubiquitous in modern and ancient turbidite systems (e.g., Kostic et al., 2010; Postma and Cartigny 2014) but have not been reported so far from subaqueous ice-contact fans (Lang and Winsemann 2013). The occurrence of cyclic steps is probably more common in confined higher-energy settings as canyons, channels and proximal channel-lobe transition zones (Fedele et al. 2017). Furthermore, the absence of cyclic steps might be related to slopes, which are probably too shallow for a sufficient reacceleration of the flow after a hydraulic jump (Lang and Winsemann 2013; Cartigny et al. 2014).

The deposition of (humpback) dunes indicates dilute transcritical to subcritical flows, which are capable of moving sand- to pebble-sized sediment and sustained enough to allow for dune migration. Although dune-scale cross-stratification has been observed in deposits of turbidity currents (e.g., Ito 2010; Sumner et al. 2012; Lang et al. 2017), it is considered rare because dune formation is suppressed by high suspension fall-out (Arnott 2012), and interpretations vary. Dune-scale cross-stratification may relate to sediment bypass (Stevenson et al. 2015) or low-density flows at channel margins (Pickering et al. 2015). Alternatively, cross-stratified deposits have been interpreted as related to short-wavelength, downflow migrating antidunes (Fedele et al. 2017; Lang et al. 2017), supercritical dunes (Fedele et al. 2017) or progradational scour fills (Arnott and Al-Mufti 2017).

5.2. Supercritical density flows in glacifluvial Gilbert-type deltas

Analysis of sedimentary facies and GPR sections from the Freden and Porta deltas clearly indicates that the delta systems are partly dominated by deposits of surge-type and sustained supercritical density flows (Fig. 10B, C). Trains of scours filled by backsets relate to the upslope migration of cyclic steps along the delta slope, and are interbedded with foreset deposits comprising subhorizontally or sinusoidally stratified pebbly sand deposited by antidunes.

Deposits of cyclic steps have been identified in previous studies of sand-rich delta successions and were interpreted as deposited by underflows related to increased discharges triggered by extreme flood events (Ventra et al. 2015) or tidal drawdown (Dietrich et al. 2016). Hughes Clarke (2016) presented direct measurements of surge-type turbidity flows and migrating cyclic steps in delta-front channels, which occurred during phases of increased discharge due to tidal drawdown. During the individual flow events, the cyclic steps migrate only a fraction of the bedform wavelength and are reactivated during the next flow event (Hughes Clarke, 2016).

The interbedding of cyclic-step and antidune deposits (Figs. 7, 8) points to supercritical flow conditions with alternating Froude numbers. These alternations of the flow conditions probably relate to variations of the discharge of the glacifluvial system on the delta plain. Meltwater discharges in such systems are subject to pronounced short-term and long-term variations and rare extreme discharge events (Marren 2005; Gilbert and Crookshanks 2009). Alternatively, the formation of cyclic steps on the delta plain may trigger autogenic variations in discharge and sediment supply, which affect the deposition of the delta foreset beds (Muto et al. 2012). Flows from the glacifluvial feeder system are sediment-laden and thus likely to evolve into hyperpycnal flows, plunging over the delta brink (Powell 1990; Russell and Arnott 2003; Plink-Björklund and Steel 2004; Winsemann et al. 2007; Ventra et al. 2015), and aggrading tractional bedforms have been laterally traced between topset and foreset beds (Ghienne et al. 2010; Girard et al. 2012). Also, Zavala and Arcuri (2016) pointed out that hyperpycnal flows represent an important class of turbidity currents, which are directly derived from the discharge of rivers in flood. Parsons et al. (2001) showed experimentally that hyperpycnal flows can be derived from very low concentration flows due to convective mixing. Furthermore, the formation of dense underflows by rapid settling of sediment from a low-density river plume was observed by Hughes Clarke (2016). In contrast, Talling (2014) discounted the formation of migrating tractional bedforms by hyperpycnal underflows, because the suspended sediment concentrations in rivers were considered to be too low.

The studied section of the Porta delta formed during slow lake-level rise (Fig. 10B). Shear-wave seismic data indicate that thick delta topset and shallow-water mouth-bar deposits are genetically linked to the high-angle Gilbert-type delta foresets (Winsemann et al. 2009). The sedimentary facies of the delta-foreset beds is dominated by deposits of supercritical surge-type density flows. The small-scale fining-upward sequences of gravelly cyclic-step deposits and sandy antidune deposits with fine-grained drapes (Fig. 8E-H) were therefore likely triggered by frequent small-volume gravitational collapses of the upper delta slope (cf., Talling 2014; Hughes Clarke 2016) during high rates of delta-front aggradation (cf., Gobo et al. 2014, 2015).

In contrast, the Freden delta mainly records deposition during lake-level highstand, when the accommodation space of the delta plain decreased or was at a minimum (Winsemann et al. 2007; Roskosch et al., 2015) (Fig. 10C). Deposits of cyclic steps are thick, occur over the entire foreset length and show less variation in grain size, pointing to more sustained density flows. Also finer-grained silt or mud drapes are absent. The finer-grained thick sandy foreset beds, deposited from migrating dunes and ripples also require sustained density flows (Winsemann et al. 2007) that may reflect plunging hyperpycnal flows (Plink-Björklund and Steel 2004; Ghienne et al. 2010; Ventra et al. 2015; Carvalho and Vesely 2017). Upslope migrating climbing ripples may be related to the hydraulic-jump zone of large-scale cyclic steps. Hyperpycnal flows are favoured by low rates of delta-front aggradation, when the accommodation space in the delta brink-zone decreased or was at a minimum and a persistent sediment bypass of the delta front occurred (cf., Gobo et al. 2015). The intercalations of coarse-grained cyclic step deposits in fine-grained delta-foreset beds with climbing-ripple cross-laminated sand (Fig. 8D) probably indicate infrequent larger slope-failure events with longer run-outs, which may have been partly related to major flood peaks (Ventra et al. 2015). Hyperpycnal flows were sustained enough to allow for the formation of migrating humpback dunes, dunes and climbing ripples on the lower foreset and toeset (cf., Mulder and Alexander 2001).

6. Conclusions

- The integration of outcrop and GPR data allows for a reconstruction of the three-dimensional geometry and larger-scale facies architecture of bedforms related to supercritical flow. Sedimentary facies can be recognised in radar facies and can be mapped to depths of up to 6 m.
- Gravel-rich basal subaqueous ice-contact fan successions consist of progradational scour fills, chute-and-pool, antidune and dune deposits, indicating deposition by waning pulses of supercritical flows. The larger-scale facies architecture is dominated by highly scoured laterally amalgamated pseudo-sheets. These pseudo-sheets are vertically stacked, indicating highly aggradational conditions.
- Sand-rich subaqueous ice-contact fan successions are characterised by deposits of isolated hydraulic jumps, antidunes and (humpback) dunes and represents deposition on the lee side of the fan-mouth bar, where the glacigenic jet flow has evolved into a sustained density flow. Facies transitions between these deposits are interpreted as related to the evolution of bedforms under spatially and temporarily changing flow conditions.
- The larger-scale facies architecture of the sand-rich subaqueous ice-contact fan deposits is characterised by lobe elements, which are interpreted to represent small-scale morphodynamic successions. Lobe elements have basal erosional surfaces associated with scours filled with backsets related to hydraulic jumps, passing upwards and downflow into antidune deposits and further into deposits of (humpback) dunes. The lobe elements form prograding and retrograding laterally offset stacks. The recurrent facies architecture of the lobe elements and their prograding and retrograding stacking pattern are interpreted as related to autogenic flow morphodynamics. The facies architecture of the sand-rich subaqueous ice-contact fan deposits is very similar to sand-rich lobe deposits of submarine fans deposited by supercritical density flows.
- Glacifluvial Gilbert-type deltas are characterised by steeply dipping foresets, comprising cyclic-step deposits, alternating with antidune deposits. Deposits of cyclic steps consist of scours infilled by massive or backset cross-stratified pebbly sand and gravel, which may form laterally extensive trains of regularly spaced scours. Perpendicular and oblique to the palaeoflow direction these deposits appear as troughs with concentric or low-angle cross-stratified infill. Downflow transitions from scour fills into sheet-like low-angle cross-stratified or sinusoidally stratified pebbly sand, deposited by antidunes, are common. Upslope migrating climbing ripples may be related to the hydraulic-jump zone of large-scale cyclic steps.
- Surge-type supercritical density flows deposited small-scale fining-upward sequences of isolated cyclic-step and antidune deposits with fine-grained drapes. In contrast, deposits of cyclic steps and antidunes related to sustained supercritical density flows are thicker, laterally more extensive and show less variation in grain size. Surge-type and sustained supercritical density flows were triggered by slope-failure events or hyperpycnal flows, respectively. Major controlling factors were accommodation-space changes in the delta-brink zone. Low accommodation space favoured sediment bypass and the formation of sustained supercritical density flows, while frequent slope failure events triggered surge-type density flows during slow lake-level rise when high rates of delta-front aggradation occurred.

Acknowledgements

Funding for this study was provided in the framework of the “Wege in die Forschung” programme of Leibniz Universität Hannover (Grant No. II-05-2014-05) and by the “Leibniz Forschungsinitiative FI:GEO”. C. Brandes and J.H. van den Berg are thanked for discussion and help with field work as well as D. Epping and R. Meyer for supporting the GPR measurements. Special thanks go to the owners of the open-pits for the permission to work on their properties. D. Hoyal and J. Fedele are thanked for discussion and sharing insights into experimental jet flows and their deposits. Constructive reviews by P. Dietrich and editor J. Knight are highly appreciated.

Appendix A. Supplementary data

Supplementary data to this article can be found online at https://doi.org/10.1016/j.sedgeo.2017.10.011.

References

Alexander, J., Bridge, J.S., Cheel, R.J., Leclair, S.F., 2001. Bedforms and associated sedimentary structures formed under supercritical water flows over aggrading sand beds. Sedimentology 48, 133–152.

Allen, J.R.L., 1984. Sedimentary Structures: Their Character and Physical Basis. Developments in Sedimentology 30. Elsevier, Amsterdam 663 pp.

Andrews, S.D., Moreau, J., Archer, S., 2016. Devonian lacustrine shore zone architecture: giving perspective to cliff exposures with ground penetrating radar. Sedimentology 63, 2087–2105.

Arnott, R.W.C., 2012. Turbidites, and the case of the missing dunes. Journal of Sedimentary Research 82, 379–384.

Arnott, R.W.C., Al-Mufti, O., 2017. Deep-marine pseudo dune cross-stratification - similar, but completely different. Journal of Sedimentary Research 87, 312–323.

Ashley, G.M., 1995. Glaciolacustrine Environments. In: Menzies, J. (Ed.), Modern Glacial Environments. Butterworth-Heinemann, Oxford, pp. 417–444.

Ashley, G.M., Southard, J.B., Boothroyd, J.C., 1982. Deposition of climbing-ripple beds: a flume simulation. Sedimentology 29, 67–79.

Bates, C.C., 1953. Rational theory of delta formation. AAPG Bulletin 37, 2119–2162.

Beres, M., Green, A., Huggenberger, P., Horstmeyer, H., 1995. Mapping the architecture of glaciofluvial sediments with three-dimensional georadar. Geology 23, 1087–1090.

Beres, M., Huggenberger, P., Green, A.G., Horstmeyer, H., 1999. Using two-and three-dimensional georadar methods to characterize glaciofluvial architecture. Sedimentary Geology 129, 1–24.

Blair, T.C., 1999. Sedimentary processes and facies of the waterlaid anvil spring canyon alluvial fan, Death Valley, California. Sedimentology 46, 913–940.

Blair, T.C., 2000. Sedimentology and progressive tectonic unconformities of the sheetflood-dominated Hell's Gate alluvial fan, Death Valley, California. Sedimentary Geology 132, 233–262.

Brandes, C., Tanner, D., 2012. Three-dimensional geometry and fabric of shear deformation bands in unconsolidated Pleistocene sediments. Tectonophysics 518-521, 84–92.

Breakspear, R., 2008. Hydrodynamics and Sedimentary Structures of Antidunes in Gravel and Sand Mixtures. PhD thesis. University of Southampton 355 pp.

Brennand, T.A., 1994. Macroforms, large bedforms and rhythmic sedimentary sequences in subglacial eskers, south-central Ontario: implications for esker genesis and meltwater re-gime. Sedimentary Geology 91, 9–55.

Bridge, J., 2009. Advances in fluvial sedimentology using GPR. In: Jol, H.M. (Ed.), Ground Penetrating Radar: Theory and Applications. Elsevier, Amsterdam, pp. 323–359.

Bristow, C.S., 1995. Facies analysis in the lower greensand using ground-penetrating radar. Journal of the Geological Society 152, 591–598.

Bristow, C.S., Jol, H.M., 2003. An introduction to ground penetrating radar (GPR) in sediments. In: Bristow, C.S., Jol, H.M. (Eds.), Ground Penetrating Radar in Sediments. Geological Society of London, Special Publication 211, pp. 1–7.

Broome, R., Komar, P.D., 1979. Undular hydraulic jumps and the formation of backlash rip-ples on beaches. Sedimentology 26, 543–559.

Carling, P.A., 1999. Subaqueous gravel dunes. Journal of Sedimentary Research 69, 534–545.

Carling, P.A., Glaister, M.S., 1987. Rapid deposition of sand and gravel mixtures downstream of a negative step: the role of matrix infilling and particle over-passing in the process of bar-front accretion. Journal of the Geological Society 144, 543–551.

Carling, P.A., Bristow, C.S., Litvinov, A.S., 2016. Ground-penetrating radar stratigraphy and dynamics of megaflood gravel dunes. Journal of the Geological Society 173, 550–559.

Cartigny, M.J.B., Ventra, D., Postma, G., van den Berg, J.H., 2014. Morphodynamics and sedimentary structures of bedforms under supercritical-flow conditions: new insights from flume experiments. Sedimentology 61, 712–748.

Carvalho, A.H., Vesely, F.F., 2017. Facies relationships recorded in a Late Paleozoic fluvio-deltaic system (Paraná Basin, Brazil): insights into the timing and triggers of subaqueous sediment gravity flows. Sedimentary Geology 352, 45–62.

Chanson, H., 2001. Current knowledge in hydraulic jumps and related phenomena. A survey of experimental results. European Journal of Mechanics - B/Fluids 28, 191–210.

Cheel, R.J., 1990. Horizontal lamination and the sequence of bed phases and stratification under upper-flow-regime conditions. Sedimentology 37, 517–529.

Clemmensen, L.B., Houmark-Nielsen, M., 1981. Sedimentary features of a Weichselian glaciolacustrine delta. Boreas 10, 229–245.

Covault, J.A., Kostic, S., Paull, C.K., Sylvester, Z., Fildani, A., 2017. Cyclic steps and related supercritical bedforms: building blocks of deep-water depositional systems, western North America. Marine Geology https://doi.org/10.1016/j.margeo.2016.12.009 (in press).

Demko, T., Hoyal, D.C., Fedele, J.J., Ghayour, K., Abreu, V., Selvam, B., Rosin, M., Postma, G., Sheets, B., 2014. Supercritical morphodynamic successions in the deposits of steep, sandy submarine fans: Ainsa and Tabernas Basins, Spain. AAPG Search and Discovery Article #90189.

Deptuck, M.E., Piper, D.J., Savoye, B., Gervais, A., 2008. Dimensions and architecture of late Pleistocene submarine lobes off the northern margin of East Corsica. Sedimentology 55, 869–898.

Dietrich, P., Ghienne, J.-F., Normandeau, A., Lajeunesse, P., 2016. Upslope-migrating bedforms in a proglacial sandur delta: cyclic steps from river-derived underflows? Journal of Sedimentary Research 86, 113–123.

Dowdeswell, J.A., Hogan, K.A., Arnold, N.S., Mugford, R.I., Wells, M., Hirst, J.P.P., Decalf, C., 2015. Sediment-rich meltwater plumes and ice-proximal fans at the margins of modern and ancient tidewater glaciers: observations and modelling. Sedimentology 62, 1665–1692.

Duller, R.A., Mountney, N.P., Russell, A.J., Cassidy, N.C., 2008. Architectural analysis of a volcaniclastic jökulhlaup deposit, southern Iceland: sedimentary evidence for supercritical flow. Sedimentology 55, 939–964.

Ehlers, J., Grube, A., Stephan, H.J., Wansa, S., 2011. Pleistocene glaciations of North Germany – new results. In: Ehlers, J., Gibbard, P.L., Hughes, P.D. (Eds.), Quaternary Glaciations – Extent and Chronology – A Closer Look. Developments in Quaternary Science 15. Elsevier, Amsterdam, pp. 149–162.

Eissmann, L., 2002. Quaternary geology of eastern Germany (Saxony, Saxon–Anhalt, South Brandenburg, Thüringia), type area of the Elsterian and Saalian stages in Europe. Quaternary Science Reviews 21, 1275–1346.

Fedele, J.J., Hoyal, D.C., Barnaal, Z., Tulenko, J., Awalt, S., 2017. Bedforms created by gravity flows. In: Budd, D., Hajek, E., Purkis, S. (Eds.), Autogenic Dynamics and Self-Organization in Sedimentary Systems. SEPM Special Publication 106. https://doi.org/10.2110/sepmsp.106.12.

Fielding, C.R., 2006. Upper flow regime sheets, lenses and scour fills: extending the range of architectural elements for fluvial sediment bodies. Sedimentary Geology 190, 227–240.

Fielding, C.R., Alexander, J., McDonald, R., 1999. Sedimentary facies from ground-penetrating radar surveys of the modern, upper Burdekin River of north Queensland, Australia: consequences of extreme discharge fluctuations. In: Smith, N.D., Rogers, J. (Eds.), Fluvial Sedimentology VI. International Association of Sedimentologists Special Publication 28, pp. 347–362.

Froude, M.J., Alexander, J., Barclay, J., Cole, P., 2017. Interpreting flash flood palaeoflow parameters from antidunes and gravel lenses: an example from Montserrat, West Indies. Sedimentology https://doi.org/10.1111/sed.12375.

Gawthorpe, R.L., Collier, R.E.L., Alexander, J., Leeder, M., Bridge, J.S., 1993. Ground penetrating radar: application to sandbody geometry and heterogeneity studies. In: North, C.P., Prosser, D.J. (Eds.), Characterization of Fluvial and Aeolian Reservoirs. Geological Society, London, Special Publication Vol. 73, pp. 421–432.

Gervais, A., Savoye, B., Mulder, T., Gonthier, E., 2006. Sandy modern turbidite lobes: a new insight from high resolution seismic data. Marine and Petroleum Geology 23, 485–502.

Ghienne, J.-F., Girad, F., Moreau, J., Rubino, J.-L., 2010. Late Ordovician climbing dune assemblages: a signature of outburst flood in proglacial outwash environments? Sedimentology 57, 1175–1198.

Gilbert, R., Crookshanks, S., 2009. Sediment waves in a modern high-energy glacilacustrine environment. Sedimentology 56, 645–659.

Girard, F., Ghienne, J.F., Rubino, J., 2012. Occurrence of hyperpyncal flows and hybrid event beds related to glacial outburst events in a Late Ordovician proglacial delta (Murzuq Basin, SW Libya). Journal of Sedimentary Research 82, 688–708.

Gobo, K., Ghinassi, M., Nemec, W., 2014. Reciprocal changes in foreset to bottomset facies in a Gilbert-type delta: response to short-term changes in base level. Journal of Sedimentary Research 84, 1079–1095.

Gobo, K., Ghinassi, M., Nemec, W., 2015. Gilbert-type deltas recording short-term base-level changes: delta-brink morphodynamics and related foreset facies. Sedimentology 62, 1923–1949.

Grasmueck, M., Weger, R., Horstmeyer, H., 2004. Three-dimensional ground-penetrating radar imaging of sedimentary structures, fractures, and archaeological features at submeter resolution. Geology 32, 933–936.

Hamilton, P.B., Strom, K.B., Hoyal, D.C., 2015. Hydraulic and sediment transport properties of autogenic avulsion cycles on submarine fans with supercritical distributaries. Journal of Geophysical Research - Earth Surface 120, 1369–1389.

Hamilton, P., Gaillot, G., Strom, K., Hoyal, D., 2017. Linking hydraulic properties in submarine distributary channels to depositional lobe geometry. Journal of Sedimentary Research 87, 935–950.

Hand, B.M., 1974. Supercritical flow in density currents. Journal of Sedimentary Petrology 44, 637–648.

Hiscott, R.N., 1994. Traction-carpet stratification in turbidites - fact or fiction? Journal of Sedimentary Research 64, 204–208.

Hornung, J.J., Asprion, U., Winsemann, J., 2007. Jet-efflux deposits of a subaqueous ice-contact fan, glacial Lake Rinteln, northwestern Germany. Sedimentary Geology 193, 167–192.

Hoyal, D.C., van Wagoner, J.C., Adair, N.L., Deffenbaugh, M., Li, D., Sun, T., Huh, C., Giffin, D.E., 2003. Sedimentation from jets: a depositional model for clastic deposits of all scales and environments. AAPG Search and Discovery Article #40082.

Hoyal, D.C., Sheets, B., Wellmer, R.W., Box, D., Sprague, A., Bloch, R., 2011. Architecture of Froude critical-supercritical submarine fans: tank experiments versus field observations. AAPG Search and Discovery Article #90124.

Hoyal, D.C., Demko, T., Postma, G., Wellmer, R.W., Pederson, K., Abreu, V., Fedele, J.J., Box, D., Sprague, A., Ghayour, K., Strom, K., Hamilton, P., 2014. Evolution, architecture and stratigraphy of Froude supercritical submarine fans. AAPG Search and Discovery Article #90189.

Hughes Clarke, J.E., 2016. First wide-angle view of channelized turbidity currents links migrating cyclic steps to flow characteristics. Nature Communications 7, 118960. https://doi.org/10.1038/ncomms11896.

Ito, M., 2010. Are coarse-grained sediment waves formed as downstream-migrating antidunes? Insights from an early Pleistocene submarine canyon on the Boso Peninsula, Japan. Sedimentary Geology 226, 1–8.

Ito, M., Saito, T., 2006. Gravel waves in an ancient canyon: analogous features and formative processes of coarse-grained bedforms in a submarine-fan system, the Lower Pleistocene of the Boso peninsula, Japan. Journal of Sedimentary Research 76, 1274–1283.

Ito, M., Ishikawa, K., Nishida, N., 2014. Distinctive erosional and depositional structures formed at a canyon mouth: a lower Pleistocene deep-water succession in the Kazusa forearc basin on the Boso Peninsula, Japan. Sedimentology 61, 2042–2062.

Jobe, Z.R., Lowe, D.R., Morris, W.R., 2012. Climbing-ripple successions in turbidite systems: depositional environments, sedimentation rates and accumulation times. Sedimentology 59, 867–898.
Jol, H.M., Smith, D.G., 1991. Ground penetrating radar of northern lacustrine deltas. Canadian Journal of Earth Sciences 28, 1939–1947.
Khadkikar, A.S., 1999. Trough cross-bedded conglomerate facies. Sedimentary Geology 128, 39–49.
Kostic, S., 2011. Modeling of submarine cyclic steps: controls on their formation, migration, and architecture. Geosphere 7, 294–304.
Kostic, S., 2014. Upper flow regime bedforms on levees and continental slopes: turbidity current flow dynamics in response to fine-grained sediment waves. Geosphere 10, 1094–1103.
Kostic, S., Sequeiros, O., Spinewine, B., Parker, G., 2010. Cyclic steps: a phenomenon of supercritical shallow flow from the high mountains to the bottom of the ocean. Journal of Hydro-Environment Research 3, 167–172.
Lang, J., Winsemann, J., 2013. Lateral and vertical facies relationships of bedforms deposited by aggrading supercritical flows: from cyclic steps to humpback dunes. Sedimentary Geology 296, 36–54.
Lang, J., Dixon, R.J., Le Heron, D.P., Winsemann, J., Le Heron, D.P., 2012. Depositional architecture and sequence strati-graphic correlation of Upper Ordovician glacigenic deposits, Illizi Basin, Algeria. In: Huuse, M., Redfern, J., Dixon, R.J., Moscariello, A., Craig, J. (Eds.), Glaciogenic reservoirs. Geological Society of London, Special Publications Vol. 368, pp. 293–317.
Lang, J., Brandes, C., Winsemann, J., 2017. Erosion and deposition by supercritical density flows during channel avulsion and backfilling: field examples from coarse-grained deep-water channel-levée complexes (Sandino Forearc Basin, southern Central America). Sedimentary Geology 349, 79–102.
Leclair, S.F., Arnott, R.W.C., 2003. Coarse-tail graded, structureless strata: indicators of an internal hydraulic jump. In: Roberts, H.H., Rosen, N.C., Filion, R.H., Anderson, J.B. (Eds.), Shelf Margin Deltas and Linked Down Slope Petroleum Systems: Global Significance and Future Exploration Potential. SEPM, Houston, pp. 817–836.
Long, D., Rajaratnam, N., Steffler, P.M., Smy, P.R., 1991. Structure of flow in hydraulic jumps. Journal of Hydraulic Research 29, 207–218.
Lønne, I., 1995. Sedimentary facies and depositional architecture of ice-contact glaciomarine systems. Sedimentary Geology 98, 13–43.
Lønne, I., Nemec, W., 2004. High-arctic fan delta recording deglaciation and environment disequilibrium. Sedimentology 51, 553–589.
Macdonald, R.G., Alexander, J., Bacon, J.C., Cooker, M.J., 2013. Variations in the architecture of hydraulic-jump bar complexes on non-eroding beds. Sedimentology 60, 1291–1312.
Mäkinen, J., 2003. Time-transgressive deposits of repeated depositional sequences within interlobate glaciofluvial (esker) sediments in Köyliö, SW Finland. Sedimentology 50, 327–360.
Marren, P.M., 2005. Magnitude and frequency in proglacial rivers: a geomorphological and sedimentological perspective. Earth-Science Reviews 70, 203–251.
Massari, F., 2017. Supercritical-flow structures (backset-bedded sets and sediment waves) on high-gradient clinoform systems influenced by shallow-marine hydrodynamics. Sedimentary Geology 360, 73–95.
Mitchum, R.M., Vail, P.R., Sangree, J.B., 1977. Seismic stratigraphy and global changes of sea-level, Part 6: stratigraphic interpretation of seismic reflection patterns in depositional sequences. In: Payton, C.E. (Ed.), Seismic Stratigraphy – Applications to Hydrocarbon Exploration. AAPG Memoir 26, pp. 117–133 Tulsa.
Mulder, T., Alexander, J., 2001. The physical character of subaqueous sedimentary density flows and their deposits. Sedimentology 48, 269–299.
Muto, T., Yamagishi, C., Sekiguchi, T., Yokokawa, M., Parker, G., 2012. The hydraulic autogenesis of distinct cyclicity in delta foreset bedding: flume experiments. Journal of Sedimentary Research 82, 545–558.
Mutti, E., Normark, W.R., 1987. Comparing examples of modern and ancient turbidite systems: problems and concepts. In: Leggett, J.K., Zuffa, G.G. (Eds.), Marine Clastic Sedimentology. Graham and Trotman, pp. 1–38 London.
Neal, A., 2004. Ground-penetrating radar and its use in sedimentology: principles, problems and progress. Earth-Science Reviews 66, 261–330.
Neal, A., Grasmueck, M., McNeill, D.F., Viggiano, D.A., Eberli, G.P., 2008. Full-resolution 3D radar stratigraphy of complex oolithic sedimentary architecture: Miami Limestone, Florida, USA. Journal of Sedimentary Research 78, 638–653.
Nemec, W., Lønne, I., Blikra, L.H., 1999. The Kregnes moraine in Gaudalen, west-central Norway: anatomy of a Younger Dryas proglacial delta in a paleofjord basin. Boreas 28, 454–476.
Normandeau, A., Lajeunesse, P., Poiré, A.G., Francus, P., 2016. Morphological expression of bedforms formed by supercritical sediment density flows on four fjord-lake deltas of the south-eastern Canadian shield (Eastern Canada). Sedimentology 63, 2106–2129.
Okazaki, H., Nakazato, H., Kwak, Y., 2013. Application of high-frequency ground penetrating radar to the reconstruction of 3D sedimentary architecture in a flume model of a fluvial system. Sedimentary Geology 293, 21–29.
Okazaki, H., Kwak, Y., Tamura, T., 2015. Depositional and erosional architectures of gravelly braid bar formed by a flood in the Abe River, central Japan, inferred from a three-dimensional ground-penetrating radar analysis. Sedimentary Geology 324, 32–46.
Parsons, J.D., Bush, J.W., Syvitski, J.P., 2001. Hyperpycnal plume formation from riverine outflows with small sediment concentrations. Sedimentology 48, 465–478.
Pickering, K.T., Hiscott, R.N., 2015. Deep Marine Systems. Wiley, Chichester 657 pp.
Pickering, K.T., Clark, J.D., Smith, R.D.A., Hiscott, R.N., Lucchi, F.R., Kenyon, N.H., 1995. Architectural element analysis of turbidite systems, and selected topical problems for sand-prone deep-water systems. In: Pickering, K.T., Hiscott, R.N., Kenyon, N.H., Ricci Lucci, F., Smith, R.D.A. (Eds.), Atlas of Deep Water Environments: Architectural Style in Turbidite Systems. Chapman and Hall, London, pp. 1–10.
Pickering, K.T., Corregidor, J., Clark, J.D., 2015. Architecture and stacking patterns of lower-slope and proximal basin-floor channelised submarine fans, Middle Eocene Ainsa system, Spanish Pyrenees: an integrated outcrop–subsurface study. Earth-Science Reviews 144, 47–81.
Plink-Björklund, P., Steel, R.J., 2004. Initiation of turbidity currents: outcrop evidence of hyperpycnal flow turbidites. Sedimentary Geology 165, 29–52.
Postma, G., Cartigny, M.J.B., 2014. Supercritical and subcritical turbidity currents and their deposits - a synthesis. Geology 42, 987–990.
Postma, G., Cartigny, M.J.B., Kleverlaan, K., 2009. Structureless, coarse-tail graded Bouma Ta formed by internal hydraulic jump of the turbidity current? Sedimentary Geology 219, 1–6.
Postma, G., Kleverlaan, K., Cartigny, M.J.B., 2014. Recognition of cyclic steps in sandy and gravelly turbidite sequences, and consequences for the Bouma facies model. Sedimentology 61, 2268–2290.
Postma, G., Hoyal, D.C., Abreu, V., Cartigny, M.J.B., Demko, T., Fedele, J.J., Kleverlaan, K., Pederson, K.H., 2015. Morphodynamics of supercritical turbidity currents in the channel-lobe transition zone. In: Lamarche, G., Mountjoy, J., Bull, S., Hubble, T., Krastel, S., Lane, E., Micallef, A., Moscardelli, L., Mueller, C., Pecher, I., Woelz, S. (Eds.), Submarine Mass Movements and their Consequences. Springer, Cham, pp. 469–478.
Powell, R.D., 1990. Glacimarine processes at grounding-line fans and their growth to ice-contact deltas. In: Dowdeswell, J.A., Scourse, J.D. (Eds.), Glacimarine Environments: Pro-cesses and Sediments. Geological Society of London, Special Publication 53, pp. 53–73.
Prelat, A., Covault, J.A., Hodgson, D.M., Fildani, A., Flint, S.S., 2010. Intrinsic controls on the range of volumes, morphologies, and dimensions of submarine lobes. Sedimentary Geology 232, 66–76.
Roksandic, M.M., 1978. Seismic facies analysis concepts. Geophysical Prospecting 26, 383–398.
Roskosch, J., Winsemann, J., Polom, U., Brandes, C., Tsukamoto, S., Weitkamp, A., Bartholomäus, W.A., Henningsen, D., Frechen, M., 2015. Luminescence dating of ice-marginal deposits in northern Germany: evidence for repeated glaciations during the Middle Pleis-tocene (MIS 12 to MIS 6). Boreas 44, 103–126.
Russell, H.A.J., Arnott, R.W.C., 2003. Hydraulic jump and hyperconcentrated-flow deposits of a glacigenic subaqueous fan: Oak Ridges Moraine, southern Ontario, Canada. Journal of Sedimentary Research 73, 887–905.
Sangree, J.B., Widmier, J.M., 1979. Interpretation of depositional facies from seismic data. Geophysics 44, 131–160.
Saunderson, H.C., Lockett, F.P.J., 1983. Flume experiments on bedforms and structures at the dune-plane bed transition. In: Collinson, J.D., Lewin, L. (Eds.), Modern and Ancient Fluvial Systems. International Association of Sedimentologists, Special Publication 6. Blackwell Science, Oxford, pp. 49–58.
Spinewine, B., Sequeiros, O.E., Garcia, M.H., Beaubouef, R.T., Sun, T., Savoye, B., Parker, G., 2009. Experiments on wedge-shaped deep sea sedimentary deposits in minibasins and/or on channel levees emplaced by turbidity currents. Part II. Morphodynamic evolution of the wedge and of the associated bedforms. Journal of Sedimentary Research 79, 608–628.
Stevenson, C.J., Jackson, C.A.L., Hodgson, D.M., Hubbard, S.M., Eggenhuisen, J.T., 2015. Deep-water sediment bypass. Journal of Sedimentary Research 85, 1058–1081.
Sumner, E.J., Talling, P.J., Amy, L.A., Wynn, R.B., Stevenson, C.J., Frenz, M., 2012. Facies architecture of individual basin-plain turbidites: comparison with existing models and implications for flow processes. Sedimentology 59, 1850–1887.
Talling, P.J., 2014. On the triggers, resulting flow types and frequencies of subaqueous sediment density flows in different settings. Marine Geology 352, 155–182.
van Wagoner, J.C., Hoyal, D.C., Adair, N.L., Sun, T., Beaubouef, R.T., Deffenbaugh, M., Dunn, P.A., Huh, C., Li, D., 2003. Energy dissipation and the fundamental shape of siliciclastic sedimentary bodies. Search and Discovery Article #40080.
Vellinga, A.J., Cartigny, M.J., Eggenhuisen, J.T., Hansen, E.W., 2017. Morphodynamics and depositional signature of low-aggradation cyclic steps: new insights from a depth-resolved numerical model. Sedimentology https://doi.org/10.1111/sed.12391.
Ventra, D., Cartigny, M.J.B., Bijkerk, J.F., Acikalin, S., 2015. Supercritical-flow structures on a Late Carboniferous delta front: Sedimentologic and paleoclimatic significance. Geology 43, 731–734.
Winsemann, J., Asprion, U., Meyer, T., Schramm, C., 2007. Facies characteristics of Middle Pleistocene (Saalian) ice-margin subaqueous fan and delta deposits, glacial Lake Leine, NW Germany. Sedimentary Geology 193, 105–129.
Winsemann, J., Hornung, J.J., Meinsen, J., Asprion, U., Polom, U., Brandes, C., Bußmann, M., Weber, C., 2009. Anatomy of a subaqueous ice-contact fan and delta complex, Middle Pleistocene, NW Germany. Sedimentology 36, 1041–1076.
Winsemann, J., Brandes, C., Polom, U., 2011. Response of a proglacial delta to rapid high-amplitude lake level change: an integration of outcrop data and high-resolution shear wave seismic. Basin Research 23, 22–52.
Wynn, R.B., Kenyon, N.H., Masson, D.G., Stow, D.A.V., Weaver, P.P.E., 2002. Characterization and recognition of deep-water channel-lobe transition zones. AAPG Bulletin 86, 1441–1462.
Yokokawa, M., Hasegawa, K., Kanbayashi, S., Endo, N., 2010. Formative conditions and sedimentary structures of sandy 3D antidunes: an application of the gravel step-pool model to fine-grained sand in an experimental flume. Earth Surface Processes and Landforms 35, 1720–1729.
Zavala, C., Arcuri, M., 2016. Intrabasinal and extrabasinal turbidites: origin and distinctive characteristics. Sedimentary Geology 337, 36–54.
Zhong, G., Cartigny, M.J.B., Kuang, Z., Wang, L., 2015. Cyclic steps along the South Taiwan Shoal and West Penghu submarine canyons on the northeastern continental slope of the South China Sea. GSA Bulletin 127, 804–824.